© 2017. Published by The Company of Biologists Ltd | Development (2017) 144, 2771-2783 doi:10.1242/dev.146647

RESEARCH ARTICLE

Inwardly rectifying potassium channels influence *Drosophila* wing morphogenesis by regulating Dpp release

Giri Raj Dahal*, Sarala Joshi Pradhan* and Emily Anne Bates‡

ABSTRACT

Loss of embryonic ion channel function leads to morphological defects, but the underlying reason for these defects remains elusive. Here, we show that inwardly rectifying potassium (Irk) channels regulate release of the *Drosophila* bone morphogenetic protein Dpp in the developing fly wing and that this is necessary for developmental signaling. Inhibition of Irk channels decreases the incidence of distinct Dpp-GFP release events above baseline fluorescence while leading to a broader distribution of Dpp-GFP. Work by others in different cell types has shown that Irk channels regulate peptide release by modulating membrane potential and calcium levels. We found calcium transients in the developing wing, and inhibition of Irk channels reduces the duration and amplitude of calcium transients. Depolarization with high extracellular potassium evokes Dpp release. Taken together, our data implicate Irk channels as a requirement for regulated release of Dpp, highlighting the importance of the temporal pattern of Dpp presentation for morphogenesis of the wing.

KEY WORDS: Fly wing morphogenesis, Dpp, BMP, Bioelectric signaling, KCNJ2, *Drosophila melanogaster*

INTRODUCTION

Dominant-negative mutations in the gene encoding the Kir2.1 potassium channel (also known as Irk) lead to Andersen-Tawil syndrome (ATS), a condition comprising diverse symptoms including craniofacial and digit patterning defects, periodic paralysis, cardiac arrhythmias and cognitive deficits (Plaster et al., 2001; Tristani-Firouzi et al., 2002; Yoon et al., 2006). Periodic paralysis, cardiac arrhythmias and cognitive deficits are likely consequences of abnormal Kir2.1 function in neurons and muscle. By contrast, it is not obvious how Kir2.1 channels regulate craniofacial and limb development.

In non-human model systems, ion channels also play important developmental roles (Bates, 2015; Levin, 2014a,b). For example, disruption of Kir2.1 function in mouse, frogs and flies results in defects in morphogenesis, suggesting a conserved developmental role for inwardly rectifying K^+ channels (Adams et al., 2016; Dahal et al., 2012; Zaritsky et al., 2000). In mice, vascular development and remodeling requires a mechanically gated cation channel (Ranade et al., 2014). In chick limb chondrocytes, inhibition of potassium channels alters the pattern of spontaneous calcium transients and reduces the percentage of cells that differentiate into cartilage (Varga et al., 2011). Further, ion channel function is necessary for dorsal closure during early embryogenesis in *Drosophila* (Hunter et al., 2014). Thus, ion channels play an essential role in morphogenesis. However, the underlying mechanisms remain unclear.

Previously, we demonstrated that deletion of Kir2.1 in mouse resulted in ATS-like phenotypes that were reminiscent of those produced by disruption of the bone morphogenetic protein (BMP) signaling pathway (Dahal et al., 2012). BMPs are members of the transforming growth factor beta (TGFβ) superfamily. We complemented the mouse studies with experiments in *Drosophila* because flies express Kir2.1 orthologs (Irk1, Irk2 and Irk3), and the role of a BMP ortholog, Decapentaplegic (Dpp), in the developing wing is well characterized. We showed that reducing the function of any Irk subunit in the wing produces phenotypes that resemble those produced by reduced Dpp signaling, such as held-out wings, thickened veins, venation pattern defects, small wings, and ablation of almost the entire wing (Adachi-Yamada et al., 1999; Chen et al., 1998; Dahal et al., 2012; de Celis, 1997; Letsou et al., 1995; Ralston and Blair, 2005; Shimmi et al., 2005; Spencer et al., 1982; Zecca et al., 1995; Zeng et al., 2007). Irk channels can be heteromeric, made up of subunits encoded by different genes (Bichet et al., 2003; Hibino et al., 2010). All three Irk subunits are expressed in the wing disc and loss of one channel subunit leads to compensatory increased expression of the other two (Dahal et al., 2012). Therefore, to mimic ATS and to eliminate the function of native Irk channels, but not other potassium channels, we expressed a dominant-negative Irk subunit, Irk2DN, in the wing. Irk2DN expression led to severe wing phenotypes, similar to those produced by dpp^{d8}/dpp^{d10} flies that selectively reduce Dpp function in the developing wing (Zecca et al., 1995). Moreover, deletion, mutation or RNAi knockdown of Irk2 function led to reduced phosphorylation of Mad (the Dpp pathway-specific intracellular mediator Smad protein) and reduced Dpp target gene expression (Dahal et al., 2012). Although this study revealed that Dpp signaling requires Irk channel function, it did not identify the underlying mechanism by which a potassium channel could influence Dpp signaling. Here, we provide evidence that loss of Irk function results in abnormal release of Dpp from the producing cell, the first step in the intracellular signaling pathway.

The Dpp signaling pathway works with other signaling pathways to establish the pattern of the fly wing (Burke and Basler, 1996; Capdevila and Guerrero, 1994; Posakony et al., 1990). In the primordial wing disc, cells along the anterior/posterior (A/P) compartment boundary produce Dpp (Nellen et al., 1996). Release of Dpp elicits a patterning response in neighboring cells by binding of Dpp to the type-2 kinase receptor Punt, which then phosphorylates a type-1 kinase receptor, Thickveins (Tkv) (Letsou et al., 1995; Nellen et al., 1994; Raftery and Sutherland, 1999). Phosphorylated Tkv (p-Tkv) phosphorylates Mad

University of Colorado Denver School of Medicine, 12800 E 19th Avenue, Aurora, CO 80045, USA.
*These authors contributed equally to this work

‡Author for correspondence (emily.bates@ucdenver.edu)

G.R.D., 0000-0003-1255-2761; S.J.P., 0000-0002-4599-5940; E.A.B., 0000-0001-6895-8942

Received 5 November 2016; Accepted 14 June 2017

Development (2017) 144, 2771-2783 doi:10.1242/dev.146647

(Wiersdorff et al., 1996). Phosphorylated Mad (p-Mad) then forms a complex with a co-Smad (Medea), enters the nucleus, affects the transcription of Dpp target genes and thereby regulates cell fate (Maduzia and Padgett, 1997; Newfeld et al., 1997; Raftery and Sutherland, 1999; Raftery et al., 1995; Sekelsky et al., 1995; Wiersdorff et al., 1996).

Multiple models have been proposed to explain how the extracellular distribution of Dpp along the A/P boundary affects signaling and consequent patterning. One model proposes that restricted diffusion of Dpp forms an extracellular gradient that designates cell fate according to Dpp concentration. GFP-tagged Dpp (Dpp-GFP) forms a gradient that mimics anti-p-Mad staining from the A/P boundary across the wing disc (Raftery and Umulis, 2012). Increasing the expression of Dpp increases the expression of Dpp target genes (Nellen et al., 1996), supporting the hypothesis that cellular fate within the wing depends on the concentration of Dpp that a cell receives (Nellen et al., 1996; O'Connor et al., 2006). More recently, the lab of Thomas Kornberg has shown that Dpp travels along specialized long filopodia (cytonemes) that synapse upon responding cells (Roy et al., 2014). Genetic disruption of cytonemes perturbs Dpp signaling (Roy et al., 2014). Thus, these data support a second model in which Dpp elicits its patterning response through contact-mediated signaling (Roy et al., 2014). Another recent concept is that the temporal pattern of presentation of Dpp-like ligands is also important for downstream signaling and responses (Sorre et al., 2014). In cell culture, pulsatile presentation of TGFβ doubles the TGFβ target transcriptional response compared with that produced by constant exposure to the same concentration of ligand (Sorre et al., 2014). The temporal dynamics of ligand presentation is important in other types of contact-mediated signaling, such as the signaling between neurons.

Here, we use the fly wing disc model to obtain mechanistic insight into Irk-dependent regulation of Dpp signaling *in vivo*. We find that Irk channels are required in the Dpp-producing cells. By monitoring release of Dpp with a fluorescently tagged version of Dpp, we record Dpp release events *in vivo*. Upon inhibition of Irk channels, the baseline fluorescence is increased and the incidence of discrete Dpp-GFP release events above baseline is reduced. Overall, our results support a model in which Irk function plays an essential role in the regulated release of Dpp and resultant tissue morphogenesis.

Irk channels regulate vesicle release in neurons and pancreatic beta cells by modulating membrane potential to influence intracellular calcium dynamics. We hypothesized that Irk channels modulate Dpp release by a similar mechanism. Calcium imaging reveals transient elevation of intracellular calcium in individual wing disc cells. Inhibition of Irk channels decreases the duration and amplitude of the calcium transients and alters Dpp release dynamics, suggesting a possible connection between intracellular calcium and Dpp release. We show that high extracellular K^+ concentrations induce Dpp release from cultured wing discs, suggesting that depolarization promotes release of Dpp. Together, our results indicate that Irk channels regulate release of Dpp and that the temporal dynamics of Dpp presentation impacts the downstream transcriptional response and resultant tissue morphogenesis.

RESULTS

Human and rat inwardly rectifying K^+ channels specifically rescue *Irk2DN* wing phenotypes

Our previous work demonstrated a role for Irk channel function in Dpp-mediated wing morphogenesis (Dahal et al., 2012). However, this previous study did not provide a cellular or mechanistic understanding of how Irk channels regulate wing disc patterning. Irk2 belongs to the Kir2 subfamily of inwardly rectifying K^+ (Kir/Irk) channels that act to maintain a stable resting membrane potential (Döring et al., 2002; Hibino et al., 2010; Luan and Li, 2012; MacLean et al., 2002). To test whether the effects produced by Irk2DN reflect a requirement for the inwardly rectifying property of the channel, we assayed for rescue of Irk2DN-induced defects by transgenic expression of different classes of Kir genes. Kir transgenes were tagged with green fluorescent protein (GFP) or Flag to allow independent confirmation of expression and membrane localization (Fig. S1). We used a wing-specific driver, *MS1096-Gal4* (*MS1096>*), that alone has no effect on wing size but can lead to mild defects (bristle transformations or mild wing venation defects) (Fig. 1A,I).

Expression of Irk2DN, which acts similarly to human ATS alleles that block Kir2 channel activity, results in severely defective rudimentary wings that consist of only the hinge region, wings of reduced size or with thickened vein tissue (Fig. 1B,C,I) (see also Dahal et al., 2012). These rudimentary wings reflect apoptosis in the late third instar larval wing disc, similar to the phenotype that results from loss of Dpp signaling (Dahal et al., 2012; de Celis, 1997, 2003). When apoptosis is blocked by expression of p53, we find that p-Mad is still reduced in those discs, indicating that reduction of Dpp signaling is upstream or independent of apoptosis (Dahal et al., 2012). Co-expression of human KIR2.1 (*KCNJ2-GFP*) with Irk2DN results in wings similar to those found upon expression of the driver alone (Fig. 1D,I). Thus, human KIR2.1 completely rescues the wing phenotypes produced by *Irk2DN*. Co-expression of another Kir channel type, rat Kir4.1 (*Kcnj10-flag*) (Hibino et al., 2010), with *Irk2DN* partially rescues the defects caused by inhibition of native Irk channels. Eleven percent of *MS1096>Irk2DN; Kcnj10-flag* wings had no detectable defects (Fig. 1E,I), whereas 35% had venation defects and 53% were severely defective (Fig. 1F,I). However, co-expression of another potassium channel type [Ork (Ork1 – FlyBase), a two-pore potassium channel], did not rescue the Irk2DN wing phenotype (Fig. 1H,I). Expression of Ork alone did not cause severe defects without expression of Irk2DN (Fig. 1G). Overall, two different mammalian Kir subfamily members, KIR2.1 and Kir4.1, rescue wing defects produced by expression of *Irk2DN*. KIR2.1 and Irk2 are both classified in the same subfamily of inwardly rectifying K^+ channels (Döring et al., 2002; Hibino et al., 2010) and KIR2.1 rescues *MS1096>Irk2DN* wing phenotypes more effectively than a member of a different subfamily, Kir4.1. These results support the view that the inwardly rectifying property of these K^+ channels plays a role in regulation of wing disc morphogenesis.

Irk2 functions in the Dpp-producing cells and is not required in Dpp-responding cells for Mad phosphorylation

Dpp is released from the producing cell and then binds to tyrosine kinase receptors on the responding cell to trigger a signaling cascade that ultimately induces target gene expression. An initial step in the signaling cascade is phosphorylation of Mad, and p-Mad can be used to as a readout of Dpp signaling. *Irk2DN* expression diminishes p-Mad, indicating a defect in Dpp signaling (Fig. 2C,E, G) (see also Dahal et al., 2012). Loss of p-Mad could be due to loss of Dpp (the signal from producing cells) or its transduction (the signaling cascade in responding cells).

To distinguish between these possibilities, we used a genetic approach and expressed a constitutively active Dpp receptor, Tkv (*tkvQD*), with or without *Irk2DN* and assayed for p-Mad. Again, we used the *MS1096* driver that results in broad expression in the center

Development (2017) 144, 2771-2783 doi:10.1242/dev.146647

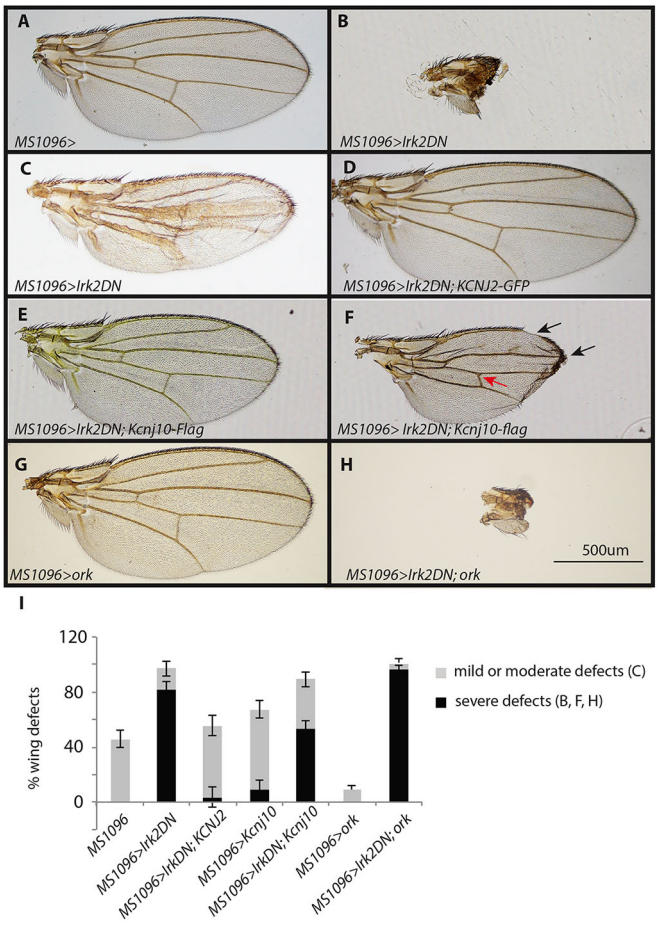

Fig. 1. The developmental role of Irk2 requires its inwardly rectifying K^+ conductance. (A) The *MS1096>* promoter drives transgene expression in larval and pupal wing discs. Wings from female control flies (*MS1096>* driver alone) develop without severe defects in size or patterning of bristles or veins. Moderate vein or bristle defects resulting from the *MS1096>* driver alone can occur but are not shown here as they were not assessed in the rescue experiments. (B) *MS1096>* promoter-driven expression of *Drosophila Irk2DN* severely affects wing formation such that only the wing hinge develops in most cases. (C) *MS1096>* promoter-driven expression of *Irk2DN* can also cause less severe wing defects, such as thickened longitudinal veins and abnormal venation pattern. (D) Human KIR2.1 (*KCNJ2-GFP*) completely rescues the defects caused by Irk2DN expression (compare with B). (E,F) In *Irk2DN*-expressing wings, rat Kir4.1 (*Kcnj10-flag*) expression fully (E) or partially (F) rescues the venation (red arrow) and bristle pattern (black arrows) defects (compare with B). (G) *MS1096>Ork* does not cause significant defects in wing development. (H) A representative rudimentary wing from an *MS1096>Irk2DN; Ork* female adult fly shows that Ork expression does not rescue defects caused by inhibition of Irk channels. (I) The percentage of wings with moderate or severe defects from three trials (mean±s.e.m.). *n*=307 *MS1096>* control, *n*=100 *MS1096> Kcnj10*, *n*=110 *MS1096>Irk2DN*, *n*=127 *MS1096>Irk2DN; Kcnj10*, *n*=100 *MS1096> Irk2DN; KCNJ2*, *n*=89 *MS1096>Irk2DN; Ork* and *n*=100 *MS1096>Ork*. Overexpression of *Irk2DN*, but not *Kcnj10*, leads to severe wing defects. Overexpression of *KCNJ2* rescues the effects of inhibition by *Irk2DN*. *Kcnj10* overexpression partially rescues the effects of *Irk2DN*. Ork overexpression does not rescue defects caused by *Irk2DN* expression.

of the wing pouch (Fig. 2A). Transgenic expression of *tkvQD* in the wing pouch results in a strong p-Mad signal throughout the wing disc (Fig. 2D,G, *n*=20). However, co-expression of *Irk2DN* had no effect on the intensity of the p-Mad signal (Fig. 2F,G, *n*=22), suggesting that Irk channels act upstream of Mad phosphorylation in the Dpp pathway. As further evidence that Irk2 is not required in Dpp-responding cells we created clones that express *Irk2DN* in the Dpp-responding cells and these showed no change in p-Mad fluorescence intensity compared with neighboring cells (Fig. 2H-K, Fig. S2, *n*=12 discs and 38 clones). These data support the view that Dpp-responding cells do not require Irk channels in a cell-autonomous manner for phosphorylation of Mad, a crucial effector of Dpp signaling.

We next tested if Irk channels function in the Dpp-producing cells for Dpp signaling. We expressed Irk2DN in the cells that produce Dpp at the A/P boundary of the wing disc (Fig. 2B) using the *dpp-gal4* (*dpp>*) driver and assessed p-Mad levels in *dpp>Irk2DN* and control (*dpp>* alone) wing discs. Inhibition of Irk channels in the Dpp-producing cells significantly reduced p-Mad in the center of the pouch of the wing disc (Fig. 2L-N, *n*=15 discs of each genotype averaged in Fig. 2L, $P<0.005$) demonstrating that Dpp-producing cells require Irk channel function for efficient presentation of the Dpp signal.

Irk channels are not required for Dpp transcription or translation

We next asked whether Irk channels function at the level of Dpp transcription, translation, processing or release. We first assessed the effects of Irk2DN on *dpp* transcription using a *dpp-lacZ* reporter. Irk2DN expression had no effect on *dpp-lacZ* expression (*n*=10 for both genotypes), nor did it affect expression of the Dpp receptor Tkv (Fig. S3, *n*=9 *MS1096>tkv-lacZ* and *n*=10 *MS1096>Irk2DN; tkv-lacZ* wing discs). We assessed effects of Irk2DN expression on intracellular Dpp protein levels using an antibody that recognizes the Dpp prodomain (Akiyama and Gibson, 2015), the portion of the Dpp proprotein that is cleaved prior to secretion. Dpp prodomain immunoreactivity in *dpp>Irk2DN* wing discs is not significantly different from that of *dpp>* wing discs (Fig. 3A-C, *n*=19 and *n*=18, respectively). This indicates that Irk2DN does not affect Dpp translation or levels of Dpp protein expression, at least as detectable by the prodomain antibody.

Next, we assayed for extracellular Dpp. Previous work (Entchev et al., 2000; Teleman and Cohen, 2000) demonstrated that the fluorescence intensity of Dpp-GFP in Dpp-producing cells provides an assessment of Dpp protein expression and distribution. Accordingly, we expressed *Irk2DN* along with *dpp-GFP* (*dpp>Irk2DN; dpp-GFP*) in the Dpp-producing cells (*dpp>*) and compared the GFP immunoreactivity with that of *dpp>dpp-GFP* wing discs. For this experiment, we prepared wing discs under conditions that do not permeabilize cellular membranes, so that the antibody would have access to extracellular but not intracellular Dpp-GFP (see Materials and Methods). Under these conditions, we find that inhibition of Irk channels in the Dpp-producing cells increases the peak fluorescence intensity and widens the A/P domain of extracellular Dpp-GFP (Fig. 3D-F, $P=0.001$ and 0.007, respectively, two-tailed *t*-test; *n*=27 *dpp>dpp-GFP* and *n*=33 *dpp>Irk2DN; dpp-GFP* wing discs). Taken together, the results suggest that *Irk2DN* expression increases the amount of extracellular Dpp and the area over which it localizes. This raises a paradox as to how to reconcile this conclusion with our data showing decreased Dpp signaling as seen by decreased p-Mad, decreased Spalt expression (Dahal et al., 2012) and by the wing patterning phenotypes (Figs 1 and 2). However, we did note that *Irk2DN* expression significantly increased the size of wing discs, which is a Dpp gain-of-function phenotype (Fig. 3G-J, Fig. S4). This could suggest a difference in the mechanism of Dpp signaling for patterning compared with wing disc size.

A possible technical explanation is that inhibition of Irk channels compromises membrane integrity, making cells more permeable to

Development (2017) 144, 2771-2783 doi:10.1242/dev.146647

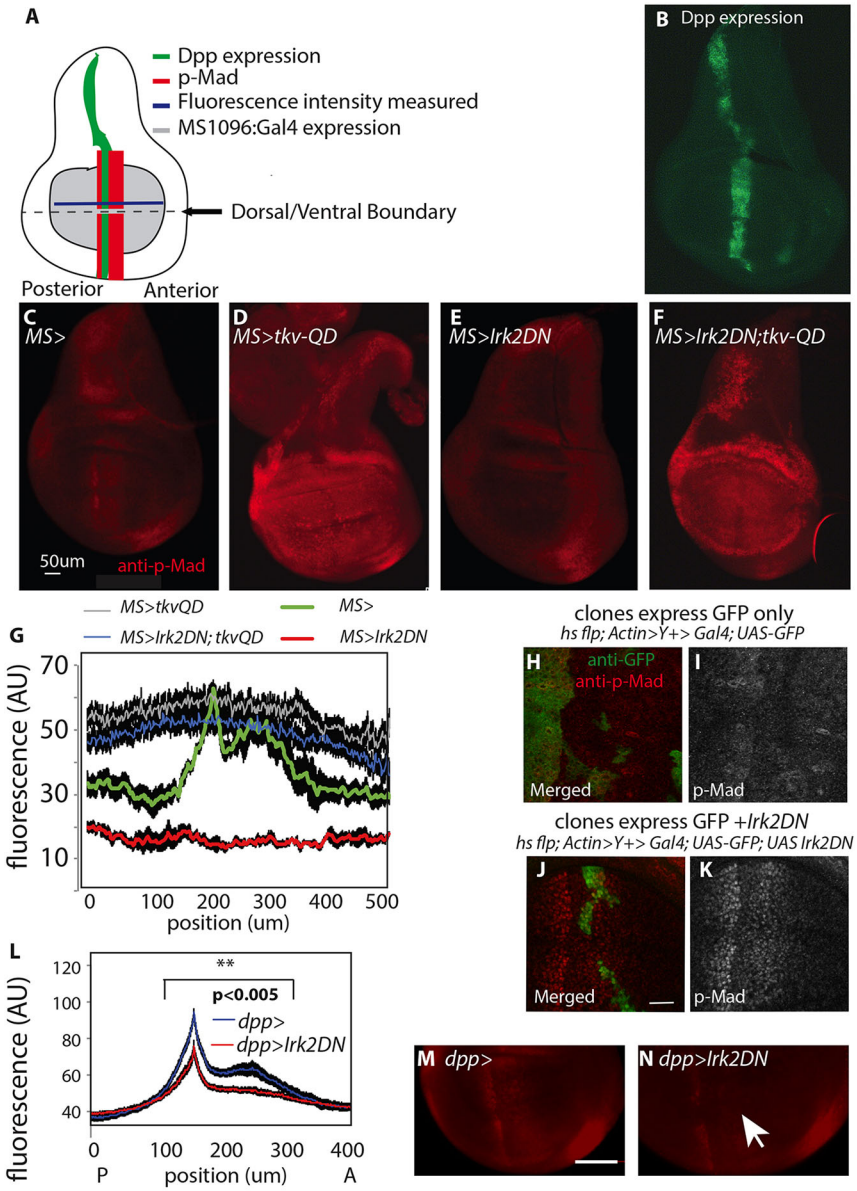

Fig. 2. Irk2 functions in the Dpp-producing cell for Dpp signaling. (A) A schematic of a wing disc showing endogenous Dpp expression, Mad phosphorylation, the region of *MS1096>* promoter-driven expression, and the region (line) where fluorescent intensity was measured. (B) A third instar larval *dpp>GFP* wing disc showing where Dpp is expressed. (C) A representative *MS1096>* (wild-type) wing disc stained with anti-p-Mad shows where Dpp signals through phosphorylation of Mad (p-Mad). (D) A representative *MS1096>tkvQD* wing disc stained with anti-p-Mad (*n*=22) demonstrates that a constitutively active Dpp receptor will cause phosphorylation of Mad throughout the wing pouch. (E) A representative *MS1096>Irk2DN* wing disc stained with anti-p-Mad (*n*=29) demonstrates that inhibition of Irk channels throughout the wing pouch inhibits Dpp signaling through p-Mad in the wing pouch. (F) A representative *MS1096>Irk2DN; tkvQD* wing disc stained with anti-p-Mad (*n*=22) shows that expression of *Irk2DN* and *tkvQD* in the same cells allows phosphorylation of Mad throughout the wing pouch, similar to *tkvQD* alone, demonstrating that Irk channel function is not required in Dpp-responding cells for Mad phosphorylation. (G) The fluorescence intensity of discs stained with p-Mad antibody peaks in the center of the wing disc, along the A/P boundary in wing discs with the *MS1096* driver alone. Mad is phosphorylated throughout the wing disc when constitutively active Tkv is expressed in the wing disc with the *MS1096* driver. Mad is not phosphorylated in the center of the wing disc when Irk2DN is expressed in the wing disc with the *MS1096* driver. Mad is phosphorylated throughout the wing disc when both Irk2DN and TkvQD are expressed in the wing disc with the *MS1096* driver. Error bars (black) represent s.e.m. (see main text for *n* values). (H) A representative wing disc stained with anti-p-Mad and anti-GFP shows clones that express GFP alone. Clones were generated using *hs flp; Actin>Y+>Gal4; UAS-GFP* flies. (I) Anti-p-Mad fluorescence in clones that express GFP alone is not significantly different from that in surrounding cells (*n*=39 clones analyzed from 12 separate wing discs). (J) A representative wing disc shows clones that express *Irk2DN*, which are marked with GFP. Wing discs are stained with anti-p-Mad (red) and anti-GFP (green) in this merged image. Clones were generated using *hs flp; Actin>Y+>Gal4; UAS-Irk2DN; UAS-GFP*. (K) Clones that express *Irk2DN* are marked with GFP. Wing discs are stained using anti-p-Mad (red) and anti-GFP (green) antibodies. Anti-p-Mad fluorescence in *Irk2DN* clones in the posterior compartment is not significantly different from that in surrounding cells. *n*=38 clones analyzed from 12 separate wing discs. The quantification of fluorescence of clones and neighbors is shown in Fig. S2. (L) Quantification of average fluorescence intensity in *dpp>Irk2DN* compared with that in control *dpp>* wing discs shows that the inhibition of Irk channels in Dpp-producing cells reduces phosphorylation of Mad in Dpp-responding cells. *n*=21 discs for each genotype. ***P*<0.005 for all points under the indicated area (bracket). Error bars (black) indicate s.e.m. (M) A representative third instar larval *dpp>* wing disc (*n*=21) stained with anti-p-Mad shows that Mad is phosphorylated in two distinct stripes along the A/P boundary. (N) A representative third instar larval *dpp>Irk2DN* wing disc (*n*=21) stained with anti-p-Mad shows that phosphorylation of Mad is reduced when Irk channels are inhibited in Dpp-producing cells (arrow). Scale bars: 50 µm in B-F; 10 µm in H-K,M,N.

Development (2017) 144, 2771-2783 doi:10.1242/dev.146647

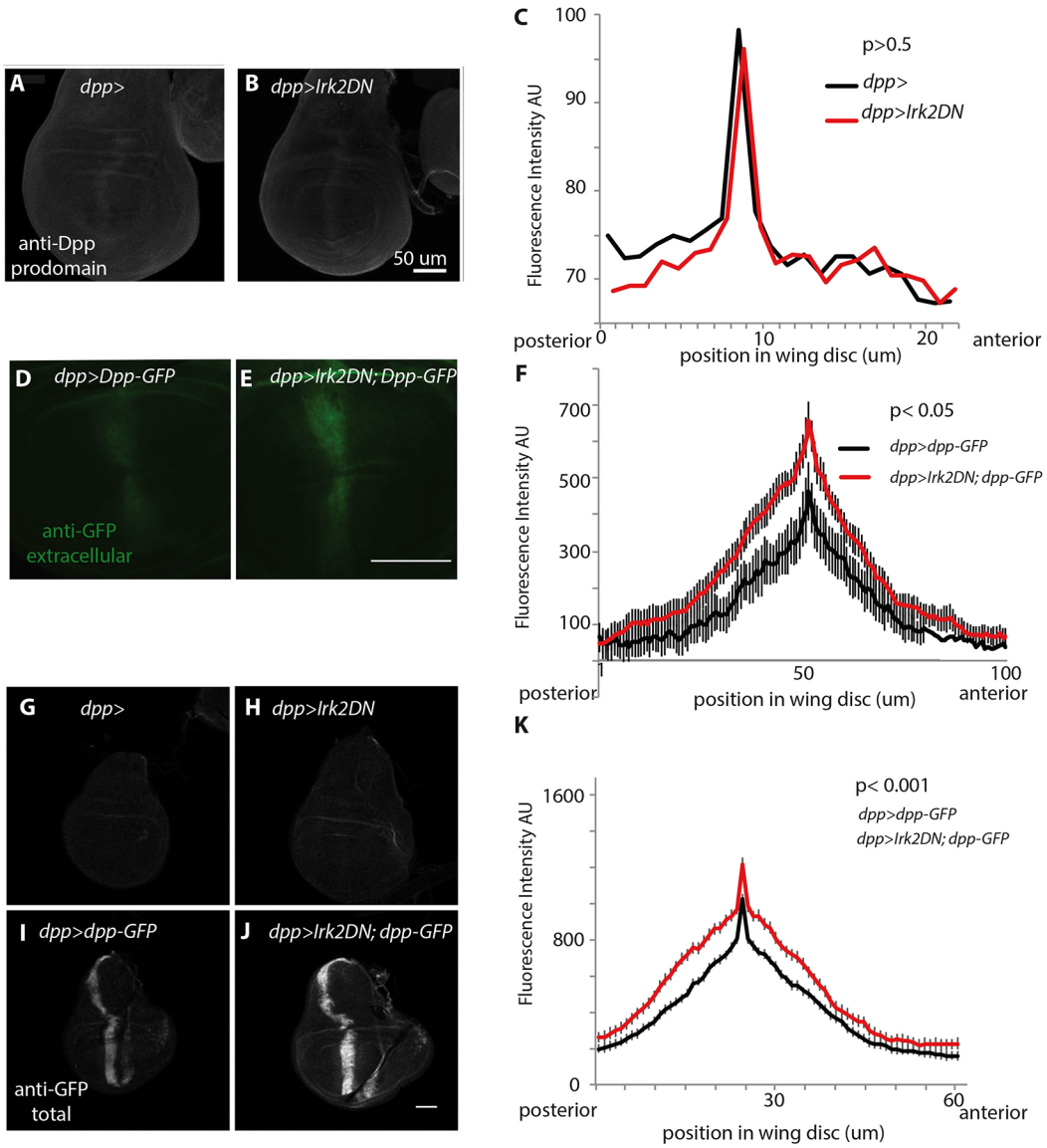

Fig. 3. Inhibition of Irk2 in Dpp-producing cells increases the intensity and expands the region of extracellular Dpp-GFP fluorescence, but does not affect the intensity or width of the intracellular Dpp prodomain. (A,B) Immunostaining with anti-Dpp prodomain antibody detects protein in both (A) *dpp>* (*n*=19) and (B) *dpp>Irk2DN* (*n*=18) third instar larval wing discs. (C) Fluorescence intensity of Dpp prodomain immunoreactivity across the third instar wing disc (144-148 AEL) from posterior to anterior shows no significant change in intracellular Dpp (*P*>0.5 by *t*-test at all positions; *n* values as A,B). (D,E) Extracellular GFP is detected by anti-GFP antibody in (D) *dpp>dpp-GFP* (*n*=38) and (E) *dpp>Irk2DN; dpp-GFP* (*n*=50) third instar larval wing discs (144-148 AEL) that were not permeabilized. (F) Fluorescence intensity of GFP immunoreactivity across the third instar wing disc (144-148 AEL) from posterior to anterior for *dpp>dpp-GFP* and *dpp>Irk2DN; dpp-GFP* (*n* values as D,E). *P*<0.05 by *t*-test in the peak fluorescent domain. Error bars represent s.e.m. (G-J) *dpp>* (*n*=17) (G), *dpp>Irk2DN* (*n*=17) (H), *dpp>dpp-GFP* (*n*=42) (I) and *dpp>Irk2DN; dpp-GFP* (*n*=36) (J) wing discs were stained with anti-GFP antibody after permeabilizing the membrane to detect total intracellular and extracellular Dpp-GFP. (K) Fluorescence intensity of GFP immunoreactivity across the third instar wing disc (144-148 AEL) from posterior to anterior for *dpp>dpp-GFP* and *dpp>Irk2DN; dpp-GFP* (*n* values as I,J). *P*<0.001 by *t*-test in the peak fluorescent domain. Error bars represent s.e.m. Scale bars: 50 µm in B; 100 µm in E; 50 µm in J.

antibodies. To test this, we performed experiments under conditions that allowed simultaneous analysis of both intracellular and extracellular Dpp-GFP. Consistent with our measures of extracellular Dpp-GFP alone, the combined levels of intracellular and extracellular Dpp-GFP fluorescence also increase in intensity and area (Fig. 3G-K). This suggests that the increased distribution and intensity of Dpp-GFP fluorescence in Irk2DN-expressing wing discs are not due to a difference in membrane permeability. We then considered the possibility that Irk channels regulate the release of Dpp.

Irk channels regulate Dpp release

To test the possible function of Irk channels in the regulation of Dpp release, we used live imaging methods in combination with expression of Dpp-GFP. These methods take advantage of the pH dependence of GFP fluorescence intensity (Bokman and Ward, 1981; Kneen et al., 1998; Miesenbock et al., 1998; Ward and Bokman, 1982). The acidic environment of the vesicular lumen quenches GFP fluorescence (Gandhi and Stevens, 2003; Paroutis et al., 2004). By contrast, the neutral environment of the extracellular space, encountered by GFP upon exocytosis, restores

Development (2017) 144, 2771-2783 doi:10.1242/dev.146647

GFP fluorescence (Fig. 4A, schematic). Thus, we monitored changes in fluorescence intensity over time to track the vesicular release of Dpp-GFP from Dpp-producing cells. First, we performed an important control to observe the unquenching of intracellular GFP: neutralizing the acidic environment of the lumen by treatment with ammonium chloride caused the Dpp-GFP fluorescence intensity to rapidly and significantly increase (Fig. S5A,B).

Next, we obtained time-lapse images of Dpp-GFP to monitor the spatial and temporal dynamics of GFP fluorescence intensity. In each *dpp>dpp-GFP* wing disc imaged we observed spontaneously appearing bright puncta of Dpp-GFP and then the fluorescence decreased in the brightest pixel of the central puncta, with a concomitant increase in fluorescence intensity of the surrounding concentric pixels (Fig. 4, Fig. S5C). The average decrease in fluorescence intensity of the central bright puncta (putative site of exocytosis) roughly equaled the sum of the increases in fluorescence intensity occurring in surrounding concentric pixels (Fig. 4B, Fig. S5C). In other words, the Dpp-GFP fluorescence spread with time consistent with GFP diffusing away from a release site, as expected for vesicular release of Dpp-GFP. Puncta that reached a threshold fluorescence above baseline were identified as discrete individual release events (Fig. 4B, Fig. S5C).

To determine whether Irk channels regulate Dpp release, we compared the changes in Dpp-GFP fluorescence intensity over time in the presence or absence of native Irk channel function. The average frequency of release events at any one particular release site in control wing discs was 1.7±0.07 events per 2 min and within the analyzed region there were 26±5 release events. Irk2DN expression reduced the incidence of discrete release events, with an average of 1.4±0.06 events per 2 min at individual release sites and 14±3 release events per analyzed region (Fig. 4B-E). However, Irk2DN increased the baseline fluorescence, quantified as the number of

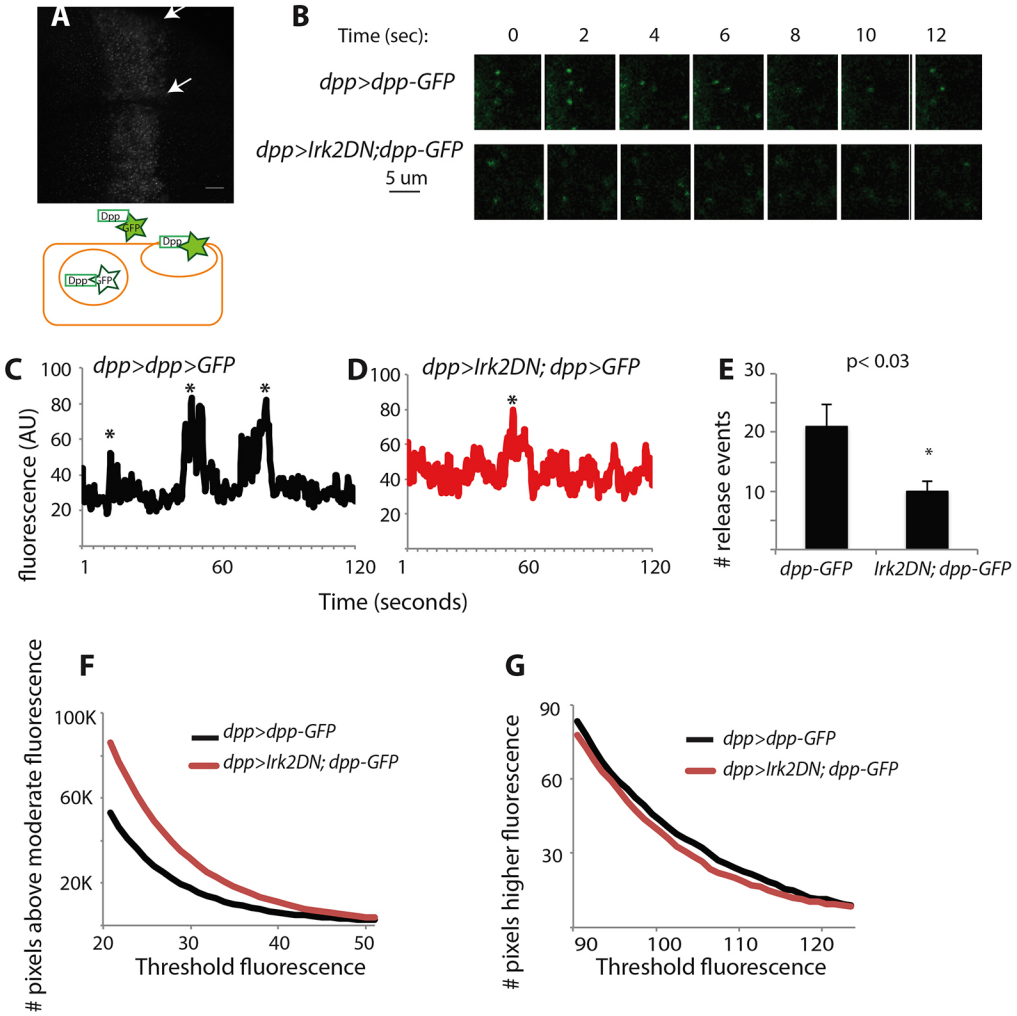

Fig. 4. Irk2 inhibition alters the properties of Dpp-GFP release. (A) A representative image showing areas where Dpp release was analyzed at the ventral edge (top) and at the D/V boundary (arrows). The schematic illustrates GFP fluorescence increasing upon release from a cell. Scale bar: 50 µm. (B) Time-lapse images show Dpp-GFP release events in a *dpp>dpp-GFP* wing disc (top) and *dpp>Irk2DN; dpp-GFP* wing disc (bottom). (C) The fluorescence profile of a representative individual release site with a three-pixel diameter in the ventral edge of a *dpp>dpp-GFP* wing disc shows two prominent Dpp-GFP release events. (D) The fluorescence profile of a representative individual release site with a three-pixel diameter in the ventral edge of a *dpp>Irk2DN; dpp-GFP* wing disc shows less discrete release events. (E) The mean±s.e.m. number of release events per 50×50 pixel region in the ventral edge over 2 min. *n*=6 *dpp>dpp-GFP* and *dpp>Irk2DN; dpp-GFP* wing discs. **P*<0.03. (F) The average number of pixels above mid-range (20-50 AU) threshold fluorescence intensity in a 50×50 pixel region at the D/V boundary of the Dpp-producing region in *dpp>dpp-GFP* and *dpp>Irk2DN; dpp-GFP* wing discs (*n*=6) at 144-148 h AEL. (G) The average number of pixels above high-range (90-130 AU) threshold fluorescence intensities in a 50×50 pixel region at the D/V boundary of the Dpp-producing region in *dpp>dpp-GFP* and *dpp>Irk2DN; dpp-GFP* wing discs (*n*=6) at 144-148 h AEL.

Development (2017) 144, 2771-2783 doi:10.1242/dev.146647

pixels with midrange fluorescence intensity (Fig. 4F), for cells located at either of the two wing disc areas analyzed [the dorsal-ventral (D/V) boundary region or the ventral edge]. There was no change in the number of pixels above high fluorescence intensity thresholds (Fig. 4G).

Overall, these data suggest that Dpp-GFP is released in discrete bursts in control wing discs. Loss of Irk2 channel function increases the baseline level of Dpp-GFP while at the same time decreasing the number of discrete high-threshold release events. This could reflect an increase in the number of release events containing smaller amounts of Dpp-GFP.

Dpp-producing cells undergo calcium spikes

In excitable cells, inhibition of Irk channels alters resting membrane potential and thereby can affect intracellular Ca^{2+} and vesicle release (Bondy et al., 1987; Braun et al., 2008; Cilz et al., 2014; Rorsman and Braun, 2013). To determine whether wing disc cells exhibit changes in intracellular calcium levels, we expressed GCaMP6-slow (GCaMP6s) with or without *Irk2DN* in the Dpp-producing cells (*dpp>Irk2DN; GCaMP6s* and *dpp>GCaMP6s*, respectively) and then imaged GCaMP6s fluorescence in wing discs over time. In the *dpp>GCaMP6s* control, we found that calcium waves propagate through the cells of the wing disc (Fig. 5A). In addition, individual *dpp>GCaMP6s* cells of the Dpp-producing zone undergo transient elevations of intracellular Ca^{2+} (Fig. 5C, top). However, in *dpp>Irk2DN; GCaMP6s* wing discs, calcium transients of both types are of reduced amplitude and are shorter in duration, in contrast to discs that express GCaMP6s alone (n=8 discs for each genotype, Fig. 5B-D). These data show that inhibition of Irk channels alters spontaneous calcium transients. Overall, Irk activity regulates the amplitude and the duration of calcium spikes in these epithelial cells of the developing embryo. To determine if depolarizing conditions can induce calcium transients, we applied high extracellular K^+ to cultured wing discs while live imaging. We found an increase in GCaMP6s fluorescence that corresponded to the time at which the K^+ solution was added, indicating that depolarization can induce calcium transients (Fig. 5E-G).

Application of high extracellular K^+ solution evokes Dpp release

Because Irk channels regulate membrane potential in several cell types (Hibino et al., 2010; Vaca et al., 1996), we hypothesized that the membrane potential may regulate the dynamics of Dpp release. To test this hypothesis, we imaged Dpp release in wing discs while we added a K^+ solution to depolarize the cells. For this assay, we used wing discs expressing Dpp tagged with a highly pH-sensitive GFP variant, Dpp-super ecliptic phlorin (Dpp-SEP), which is less fluorescent at low pH than GFP and therefore has a better signal to noise ratio. Addition of K^+ solution led to an increase in the fluorescence of Dpp-SEP in *dpp>dpp-SEP* wing discs (Fig. 5H-J). The ability of high K^+ to trigger elevations of intracellular calcium as well as the release of Dpp-SEP implicates membrane potential as a regulator of these physiological processes. Further, these data suggest that Irk channels regulate Dpp release through impacting membrane potential (Fig. 6).

DISCUSSION

Irk channels regulate resting membrane potential in excitable cells and thus can modulate how readily a neuron fires an action potential, a muscle contracts, or a pancreatic beta cell secretes insulin (Bondy et al., 1987; Braun et al., 2008; Cilz et al., 2014; Hibino et al., 2010; Riz et al., 2015; Rorsman and Braun, 2013; Vaca et al., 1996). A mechanism explaining how Irk channels could impact morphogenesis was less clear. The results reported here provide insights into the underlying mechanism. First, Irk2DN-induced wing defects are most efficiently rescued by KIR2.1, a strong inward rectifier, whereas Kir4.1, a moderate inward rectifier, partially rescues wing phenotypes (Fig. 1). By contrast, an open rectifier potassium channel does not rescue Irk2DN wing phenotypes. We conclude that the inward rectifying property is important for the developmental function of Irk channels. The inward rectifying property is important for setting resting membrane potential, and when this type of channel is inhibited in other cell types they become depolarized. Second, we show that Irk channels function in the Dpp-producing cells and are not required cell-autonomously for transmission of the Dpp signal (Fig. 2). Third, we show a difference in Dpp distribution and the dynamics of Dpp release in Irk2DN compared with control wing discs (Figs 3 and 4). Fourth, we show that inhibition of Irk channels decreases the duration and amplitude of native calcium activity (Fig. 5). Finally, we show that depolarization with extracellular potassium can induce Dpp release (Fig. 5). Together, these data lead us to hypothesize that Irk channels regulate membrane potential to mediate calcium-dependent secretion of Dpp (Fig. 6). Because we do not see a reduction in the expression or distribution of Dpp, we hypothesize that changes in the temporal dynamics of Dpp presentation account for reduced p-Mad, altered transcriptional output and disrupted morphogenesis.

Our data show that ion channels modulate cell signaling and cell fate specification in wing development in *Drosophila*, adding to a body of work demonstrating a role for bioelectric signaling in embryonic processes in vertebrates and invertebrates (Bates, 2015; Levin, 2012, 2014a). Indeed, mutations that disrupt Kir2.1 or the CaV1.2 calcium channel cause similar developmental phenotypes, suggesting that at least some developmental processes in vertebrates require ion channel function and could share a bioelectric mechanism (Plaster et al., 2001; Splawski et al., 2004; Swapna and Borodinsky, 2012; Tristani-Firouzi et al., 2002). Furthermore, Michael Levin's group demonstrated that disruption of bioelectric signaling can induce ectopic eyes and limbs, reverse the left-right or A/P axes, disrupt patterning of *Xenopus* craniofacial development, and augment regenerative properties, showing that bioelectric signaling is an important driver of morphogenesis across species (Adams et al., 2016; Levin, 2012, 2014a,b; Pai et al., 2012; Tseng et al., 2010).

Here we used Dpp-GFP as a proxy to probe the distribution of extracellular Dpp and its pattern of release, similar to studies by others (Teleman and Cohen, 2000). Endogenous Dpp forms a gradient (Raftery and Umulis, 2012), as does Dpp-GFP (Fig. 3) (Teleman and Cohen, 2000). Contrary to what is expected for reduced Dpp signaling, inhibition of Irk channels alters the gradient by expanding its width and increasing the intensity of Dpp-GFP fluorescence. At first glance our data are counterintuitive in showing that Irk2DN increases the peak intensity of Dpp-GFP (Fig. 3) and increases the baseline noise of Dpp-GFP fluorescence, but decreases p-Mad and Dpp signaling. This contradiction led us to hypothesize that Irk channels affect the temporal dynamics of Dpp exposure rather than the spatial distribution of Dpp. Using live imaging of Dpp-GFP fluorescence, we find that Dpp-GFP release occurs in bursts. Inhibition of Irk channels alters the dynamics of Dpp release, and fewer release events above baseline noise are observed (Fig. 4). However, there is more variation in the baseline fluorescence when Irk channels are inhibited, which could reflect release events that occur more constantly but with less Dpp-GFP

Development (2017) 144, 2771-2783 doi:10.1242/dev.146647

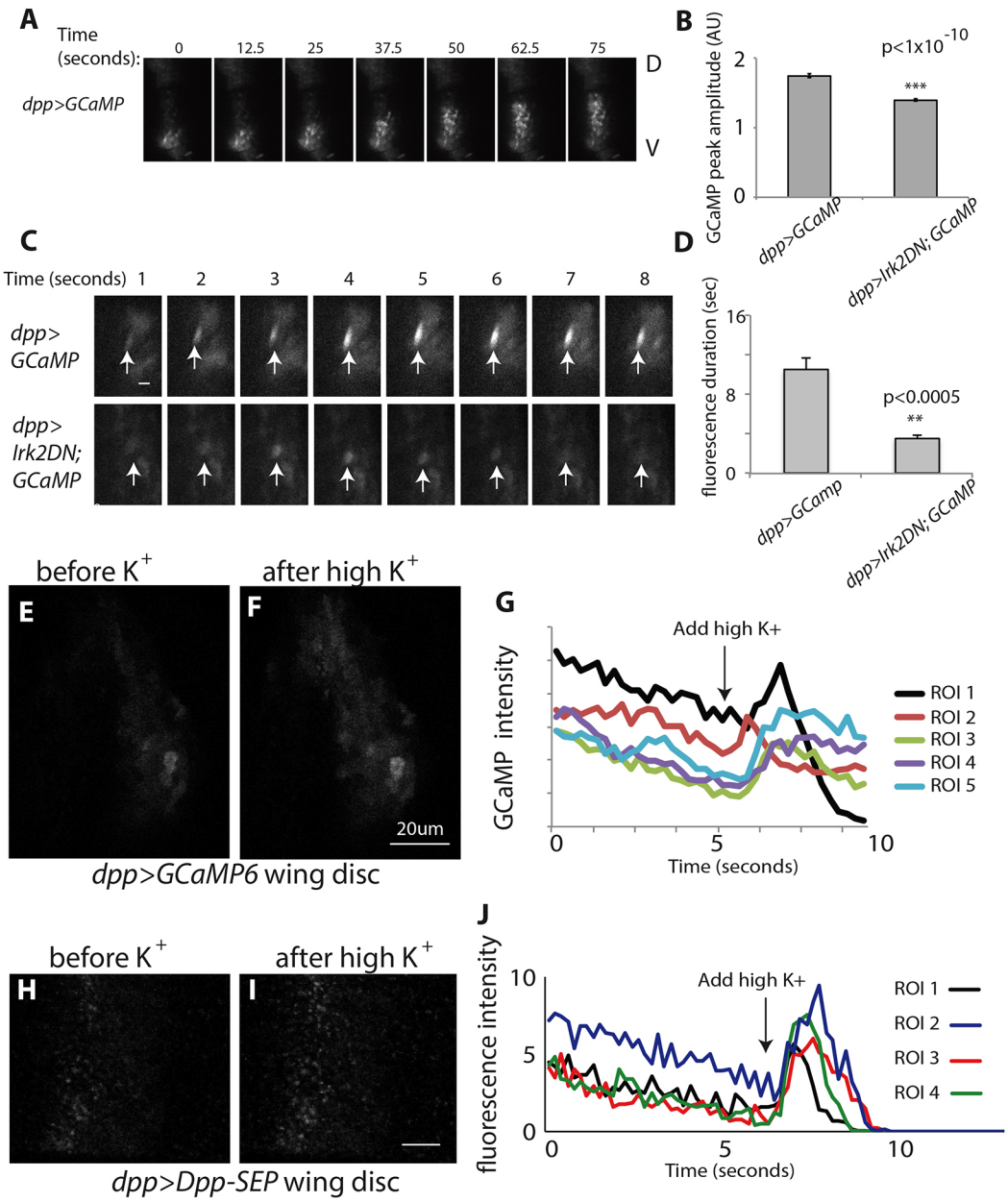

Fig. 5. The wing disc displays spontaneous increases in intracellular calcium levels. (A) Representative time-lapse images of a *dpp>GCaMP6s* wing disc showing a wave of changes in GCaMP6s fluorescence from ventral to dorsal over time (*n*=9 discs of each genotype). (B) Expression of *Irk2DN* significantly reduces the amplitude of peak GCaMP6s fluorescence, indicating that there is less variation in intracellular calcium levels when *Irk2DN* is expressed. Amplitude was determined by dividing maximum fluorescence by minimum fluorescence of each cell. *N*=261 cells selected from *n*=9 *dpp>GCaMP6s* discs and *N*=202 cells selected from *n*=11 *dpp>Irk2DN; GCaMP6s* discs. Error bars represent s.e.m. (C) Representative time-lapse images of *dpp>GCaMP6s* (top) and *dpp>Irk2DN; GCaMP6s* (bottom) wing discs show changes in GCaMP6s fluorescence in an individual cell (arrowed) of the wing disc over time. 480 images were taken at 4 Hz for a total of 2 min. GCaMP6s activity was assessed in 9 discs for each genotype. Scale bar: 10 µm. (D) Expression of *Irk2DN* significantly reduces the duration of peak GCaMP6s fluorescence. Error bars represent s.e.m. (E) A representative (out of 5 discs) image of a *dpp>GCaMP6s* wing disc shows GCaMP6s fluorescence in normal (5 mM) K^+ solution 1 s before addition of high K^+ solution. (F) The same representative *dpp>GCaMP6s* wing disc shows an increase in GCaMP6s fluorescence when the K^+ concentration is increased to 100 mM to depolarize cells of the wing disc. (G) An increase in GCaMP6s fluorescence is seen in multiple regions of interest (ROI) when the K^+ concentration is increased to 100 mM. Images were taken every 250 ms. (H) A representative (out of 6 discs) image of a *dpp>dpp-SEP* wing disc shows Dpp-SEP fluorescence in normal (5 mM) K^+ solution. (I) The same representative *dpp>dpp-SEP* wing disc shows an increase in Dpp-SEP fluorescence when the K^+ concentration is increased to 100 mM to depolarize the cells. Scale bar: 25 µm. (J) An increase in Dpp-SEP fluorescence is seen in multiple regions of interest when K^+ is increased to 100 mM. Images were taken every 250 ms.

released per event. Thus, inhibition of Irk channels would increase the frequency of Dpp release, changing Dpp release from discrete pulses to an essentially constant secretion of Dpp. Inhibition of Kir channels depolarizes cells, increases intracellular calcium and increases the secretion from excitable cells (Bondy et al., 1987; Braun et al., 2008; Cilz et al., 2014; Misler et al., 1992; Riz et al., 2015; Rorsman and Braun, 2013), and we hypothesize that a similar mechanism could be at play in the *Drosophila* wing disc.

We propose that alteration of Dpp dynamics reduces developmental signaling. This is consistent with the idea that

Development (2017) 144, 2771-2783 doi:10.1242/dev.146647

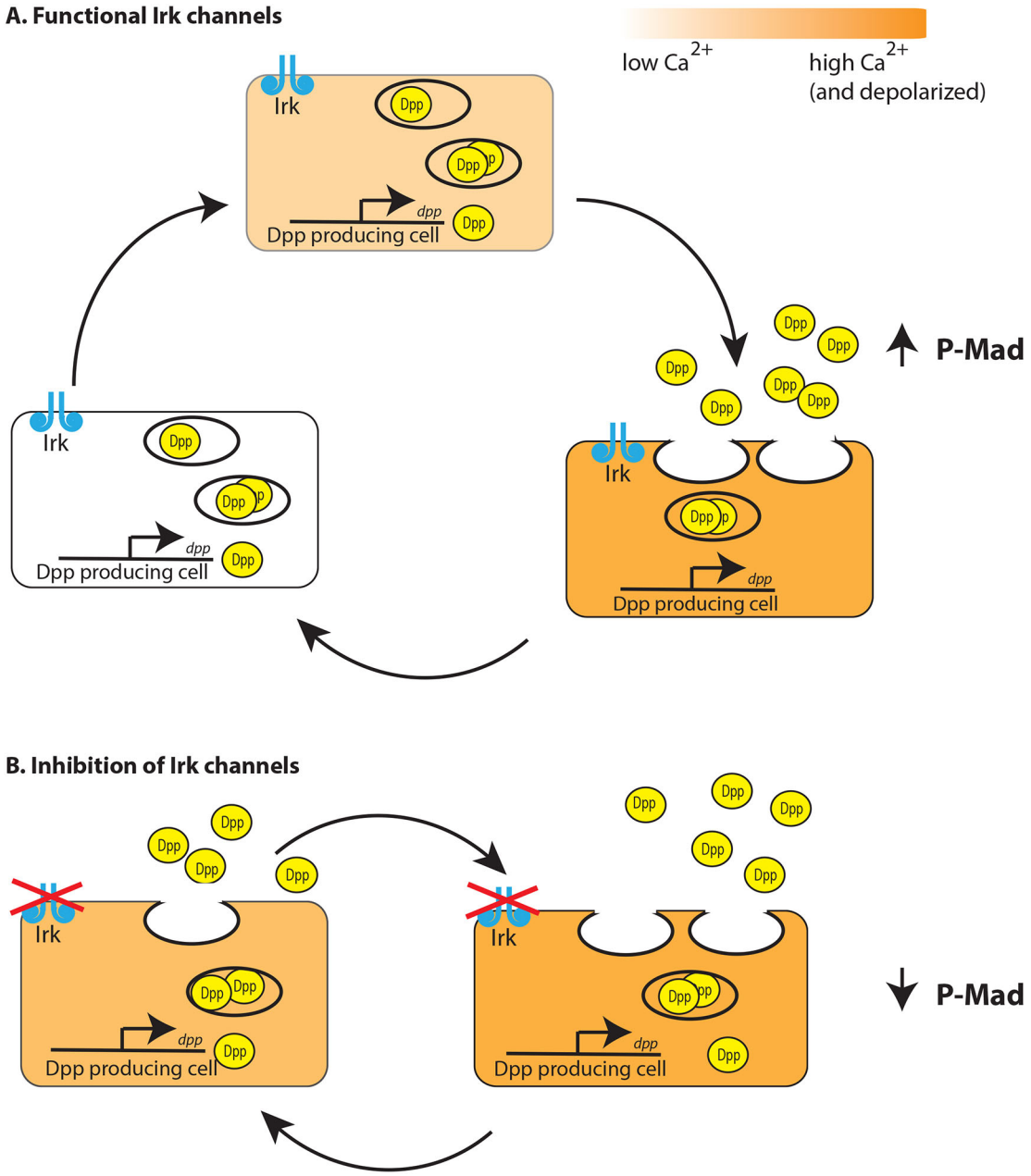

Fig. 6. Model for the mechanism by which Irk channels influence Dpp secretion. (A) When Irk channels are functional, Dpp-producing cells depolarize causing an increase in intracellular calcium and secretion of Dpp. Following secretion, the cells repolarize and intracellular calcium is restored to normal levels. This results in pulses of Dpp secretion. Pulsatile Dpp exposure is efficiently transmitted as phosphorylation of Mad in Dpp-responding cells. (B) When Irk channels are inhibited, Dpp-producing cells remain depolarized and intracellular calcium remains high. Fluctuations in intracellular calcium are not as profound. Under these conditions, vesicles containing Dpp may fuse with the membrane indiscriminately, resulting in smaller packages of Dpp being released more frequently rather than large bursts. This could result in reduced phosphorylation of Mad in the Dpp-responding cell.

temporal release of Dpp is important for developmental signaling. Siggia and colleagues used embryonic stem cells and a microfluidics *in vitro* system to show that the temporal pattern of exposure to a Dpp-like ligand (TGFβ) drastically affects the transcriptional readout of responding cells (Sorre et al., 2014). Compared with constant exposure to ligand, pulsed exposure to the TGFβ ligand doubles the transcriptional response and more effectively influences cell fate (Sorre et al., 2014). Here, by imaging cells *in situ*, we find that Dpp-GFP release also occurs in a pulsatile manner and that loss of Irk channel function alters the temporal pattern of Dpp presentation. Such a change in the temporal pattern of Dpp release would have four major consequences. First, constant secretion of Dpp would increase the amount of extracellularly localized Dpp, as we found (Fig. 3). Second, an essentially constant release of Dpp would prevent adequate refilling of vesicles with Dpp, resulting in small-amplitude Dpp-GFP release events that might escape detection and appear as a noisy baseline, consistent with our data (Fig. 5). Third, the temporal pattern of vesicular release of Dpp would change from bursts to constant, with potential effects on signaling efficacy. Fourth, reducing the function of Irk channels (by deficiency, RNAi, P-element insertion or Irk2DN expression) causes phenotypes that are typical for reduced

Development (2017) 144, 2771-2783 doi:10.1242/dev.146647

Dpp signaling: thickened veins, crossvein defects, and reduction in wing size (Dahal et al., 2012).

Our studies reveal that Irk channel inhibition in wing discs also alters intracellular calcium activity. Whether and how these effects conspire toward a common mechanism merits further study. One possibility is that intracellular Ca^{2+} dynamics regulates Dpp release. The calcium recordings and the live imaging of Dpp-GFP release dynamics were 2 min in duration, imaging four times per second, so that we could note similarities in frequency. However, each of these measurements occurs at a different scale. The Dpp-GFP release is measured at the size of the vesicle (like a synapse), whereas the GCaMP6s signals are measured at the scale of cells. Therefore, the frequency cannot be directly compared between these experiments. That said, the average frequency of Dpp-GFP release events in control wing discs is 1.7 events per 2 min and the average number of GCaMP6s events in a cell per 2 min is close to that, at 2.3. In Irk2DN-expressing wing discs, release events have an average frequency of 1.4 events per 2 min and 1.9 GCaMP6s events per 2 min (Figs 4 and 5). Furthermore, an increase in extracellular K^+ concentration induces Dpp release (Fig. 5). Together, these data support the hypothesis that innate changes in intracellular calcium regulate secretion of Dpp in the context of the wing disc (Fig. 6).

Membrane potential plays a key role in regulating BMP secretion in other systems. At the *Drosophila* neuromuscular junction, electrical activity regulates the release of a different BMP ligand, Glass bottom boat (Gbb), from postsynaptic muscle fibers to stimulate growth and development of the presynaptic boutons (Baines, 2004; Berke et al., 2013; James et al., 2014; Xiao et al., 2013). A Gbb receptor, Wit, and its downstream effector Mad are both required in the presynaptic neuron for retrograde BMP signaling to strengthen synapses (Berke et al., 2013). Interestingly, the induction of boutons by Gbb requires correct localization of functional ion-conducting glutamate receptors to the synapse (Sulkowski et al., 2014). Correctly localized but non-functional glutamate receptors do not support the effects of Gbb on boutons (Sulkowski et al., 2014). In another example, interactions between electrical activity and BMP signaling affect the balance between excitatory and inhibitory spinal neuron differentiation in the frog (Swapna and Borodinsky, 2012). Our data present the possibility that Irk channels modulate membrane potential and intracellular calcium levels to regulate BMP release from wing disc cells, as is the case in other cell types.

Several ion channels, including calcium, sodium, potassium and chloride channels, are expressed in the third instar larval discs, some of which have been shown to be specifically expressed in the wing disc (Contrino et al., 2012; Doherty et al., 1997; Klebes et al., 2002). The identification of the repertoire of ion channels that affect morphogenesis of the wing disc has the potential to reveal additional channels required for the regulation of Dpp signaling.

MATERIALS AND METHODS

Drosophila stocks and wing disc preparation

The Bloomington *Drosophila* Stock Center (BDSC) supplied many fly lines, including: *UAS-Hsap-KCNJ2-GFP.EGFP7* (BDSC #6595); *UAS-GFP* w^{1118}*; P{*w^+*:UAS-GFP.nls}8* (BDSC #4776) and *w[1118]; PBac{y[+mDint2] w[+mC]=2xUAS-IVS-GCaMP6s}VK* (BDSC #42749). From the same source, we also obtained *ry506P(PZ)hhP30, cn1P(PZ)dpp10638/CyO; ry506*, *tkv(y1w67c23); P(lacW)tkvk16713/(CyO)* and *w*; wgSp-1/CyO; P{GAL4-dpp.blk1}40C.6/TM6B, Tb1*. *w*,P{UAS-tkv.Q253D.Nb}3/TM3,Sb1Ser1* (Burke and Basler, 1996) was a gift from Dr R. E. Ward (University of Kansas, Lawrence, USA). *hs flp; Actin>Y+>Gal4* was provided by Drs L. and Y.-N. Jan (University of California San Francisco, USA). Dr E. Ferguson (University of Chicago, USA) supplied *UAS-dpp-GFP/TM3,Sb*.

All flies were kept in an incubator at 25°C unless otherwise noted. Roughly equal numbers of male and female adult flies were assessed for wing defects in the rescue experiments represented in Fig. 1. All wing discs were collected from third instar larvae of ages 144-148 h after egg lay (AEL). To ensure that wing discs of both genotypes were healthy, we used terminal deoxynucleotidyl transferase (TdT) dUTP nick-end labeling (TUNEL) Dead End Fluorometric TUNEL system (Promega, REFG3250) to assess apoptosis in *dpp>GFP* and *dpp>Irk2DN; GFP* wing discs. We found no apoptosis for either of these conditions (Fig. S6). In addition, to assess the health of the cells, we determined that the GFP fluorescence of *dpp>Irk2DN; GFP* was not obviously decreased compared with *dpp>GFP* wing discs, as it would be if the cytoplasm had become acidic as in a dying cell. Larvae sex was not assessed before wing disc dissection. Approximately equal numbers of male and female flies of these genotypes eclose. Therefore, we believe that both male and female wing discs are represented in all of our data.

Generation of Kir4.1 transgenic fly strains

Kcnj10-flag was amplified from a plasmid containing Flag-tagged rat *Kcnj10* (gift from Dr M. Levin, Tufts University, Medford, USA) using primers: forward 5′-GCGCGGAATTCAACATGACATCAGTTGC-3′ and reverse 5′-CCGCTCGAGTCATTCACTTGTCATCG-3′. The product was cloned into a pUAST vector (Lily Jan lab, University of California, San Francisco, CA, USA) between *Eco*RI and *Xho*I sites. The construct was submitted to BestGene for generation of transgenic fly lines. For channel rescue experiments we used line eight, in which *UAS-Kcnj10-flag* was integrated into the third chromosome. We confirmed expression of all *UAS* constructs in transgenic flies with RT-PCR for *Kcnj10*, *KCNJ2* and *Irk2DN* (Fig. S1).

Calcium imaging

Eggs were collected during a 4 h period. *dpp>GCaMP6s* (*BL42749*) and *dpp>Irk2DN; GCaMP6s* wing discs were dissected 144-148 h AEL in Shields and Sang M3 Insect Medium (Sigma-Aldrich, S3652) and transferred to Sylgard (Dow Corning) wells on glass slides containing M3 medium. The peripodial membrane of the wing discs faced the coverslip. GCaMP6s signals were acquired within 15 min of preparation at 4 Hz for 5 min, using a 488 nm laser and a Marianas inverted spinning disc microscope (Intelligent Imaging Innovations). Custom-written MATLAB (MathWorks) probes, kindly provided by Dr William J. Betz (Department of Physiology, University of Colorado Denver Anschutz Medical Campus, CO, USA), were used for analysis of calcium activity and can be obtained upon request to the corresponding author. Cells with the highest variance were identified and selected as regions of interest. The fluorescence profile for the region of interest was measured and plotted over 5 min. Calcium spikes were quantified for each disc (n=8 discs for each genotype). Samples were excluded from analysis if the wing disc moved during imaging or excessive photobleaching prevented assessment of the signal.

Clone generation

hs flp; Actin>Y+>Gal4, UAS-GFP/CyO virgin female flies were crossed with *UAS-Irk2DN/CyO-GFP* males. Clones were generated by heating the larvae for 1 h in a 37°C waterbath 1 day AEL. Third instar larvae were dissected and stained for p-Mad as described below. Fiji/ImageJ software (http://fiji.sc/Fiji) was used to measure fluorescence intensity in a rectangular region of interest inside a clone as compared with a neighboring region of the same size parallel to the A/P boundary. A two-tailed t-test was used to compare the fluorescence intensities within and outside of clones.

Immunohistochemistry

To control the age of the larvae, we restricted egg collection to a 4 h period. Discs were dissected 144-148 h AEL. Discs were isolated from larvae in ice-cold PBS. Isolated discs were fixed in 4% paraformaldehyde in PBS for 30 min, washed with PBS and then permeabilized using 0.3% Triton X-100 followed by treatment with 0.1% saponin. The samples were blocked in

Development (2017) 144, 2771-2783 doi:10.1242/dev.146647

blocking buffer (3% BSA, 5% goat serum, 0.1% saponin in 1× PBS) for 1 h at room temperature. Primary antibody diluted in blocking buffer was added to the samples and incubated at 4°C overnight. Samples were washed with 0.1% saponin in PBS and incubated in secondary antibody for 2 h at room temperature and washed again with 0.1% saponin. Finally, samples were mounted in Vectashield mounting medium (Vector Labs). Primary antibodies included mouse anti-β-galactosidase [1:50; Developmental Studies Hybridoma Bank (DSHB)], rabbit anti-p-Mad (1:20; Cell Signaling, 9516S, lot 60) and rabbit polyclonal anti-DYKDDDDK-tag pAb (1:1000, Genscript, A00170). Secondary antibodies included Alexa Fluor 488 goat anti-mouse IgG (1:700; Invitrogen, A11001), goat anti-mouse IgG Cy5 (1:200; Millipore, AP124S) and goat anti-rabbit IgG Cy3 (1:700; Invitrogen, A10520, lot 1387825). Imaginal discs from third instar *MS1096>KCNJ2-GFP* control and *MS1096>Irk2DN; KCNJ2-GFP* larval discs were stained with mouse monoclonal GFP antibody (1:200; Santa Cruz Biotechnology, SC-101525) and rat DCAD2 antibody (1:100; DSHB). *MS1096>Kcnj10-flag* and *MS1096>Irk2DN; Kcnj10-flag* discs were stained with mouse anti-Flag (1:500; Sigma-Aldrich, F1804-50UG, lot SLBK1345V) and rat anti-DCAD2 (1:100; DSHB). The wing discs were co-stained with secondary antibodies conjugated with Alexa Fluor 488 and Cy5.

The rabbit anti-Dpp prodomain antibody (Akiyama and Gibson, 2015) (gift from Matthew Gibson, Stowers Institute, Kansas City, USA) was diluted 1:100 in Can Get Signal B (Toyobo) containing 0.1% Triton X-100, 10% normal goat serum and anti-rabbit Cy3 (1:500; Life Technologies). The discs were mounted in PermaFluor mountant (ThermoScientific). Confocal *z*-stack images of Dpp-stained wing discs were taken with a Zeiss LSM 780 confocal microscope. Control and experimental samples were imaged on the same day with the same settings. The fluorescence intensity was measured from posterior to anterior in four lines across the A/P boundary, with two above and two below the D/V boundary using Fiji/ImageJ software. To average fluorescence intensity profiles of all samples, the central Dpp-stained region was aligned at the peak intensity. Data were normalized to the minimum baseline intensity.

For staining extracellular Dpp-GFP, third instar wing discs were collected from larvae at 130-134 h AEL in Schneider 2 culture medium (Life Technologies) and incubated in mouse monoclonal anti-GFP (1:50) for 1 h on ice. Discs were washed with PBS and fixed in 4% paraformaldehyde. Subsequent staining procedures followed previously described protocols (Strigini and Cohen, 2000). Alexa Fluor 488 goat anti-mouse IgG (1:700; Invitrogen) was used as the secondary antibody.

Fluorescence profiles of single images

Control and experimental wing discs were imaged on the same day with the same settings. The maximum intensity projection was used for fluorescence intensity analysis using Fiji/ImageJ software. Immunofluorescence of wing discs was measured in four lines across the disc immediately dorsal of the D/V boundary as depicted in Fig. 2A. Fluorescence was measured in four lines for each disc from posterior to anterior across the wing disc. To normalize to the background, we used the anchor point method, setting the anchor point as the minimum of the posterior trough of fluorescence intensity (Brooks et al., 2012).

Assessment of GFP quenching in the wing disc

Wing discs from third instar *dpp>dpp-GFP* and *dpp>Irk2DN; dpp-GFP* larvae (144-148 h AEL) were isolated and placed in PBS on a Premium cover glass (Fisher Scientific) with the peripodial side facing down. Maximum intensity projection images were acquired from confocal *z*-stacks (Zeiss LSM 780 confocal microscope) before and after addition of ammonium chloride to a final concentration of 20 mM. The same settings were used to acquire confocal images before and 1 min after addition of ammonium chloride.

Live imaging of Dpp-GFP release

Wing discs were dissected and transferred to Sylgard wells containing HL3.1 saline solution (70 mM NaCl, 5 mM KCl, 1.5 mM $CaCl_2$, 4 mM $MgCl_2$, 10 mM $NaHCO_3$, 5 mM trehalose, 115 mM sucrose and 5 mM HEPES, pH 7.4) (Jan and Jan, 1976; Stewart et al., 1994) with the peripodial side facing away from the slide. Thus, upon applying a coverslip, the disc can be imaged from the apical side. Images were taken with a Zeiss LSM 780 confocal microscope every 250 ms over 120 s. Control and experimental samples were imaged using the same confocal settings. For analysis of Dpp-GFP fluorescence, images were loaded into MATLAB as uncompressed AVI files and analyzed using custom-written programs (kindly provided by Dr William J. Betz). Two regions of 50×50 pixels were selected for analysis. The first was just anterior to the Dpp-producing A/P boundary and ventral of the D/V boundary. The second was just anterior to the ventralmost Dpp-producing cells. Pixels with the highest variance in fluorescence throughout the file were identified and selected as a region of interest with a radius of three pixels. The fluorescence profile of the brightest pixel within the region of interest was plotted over time. Release events were identified as a rise in fluorescence significantly above baseline. Imaging files were excluded from analysis if the wing disc moved during imaging.

High potassium-evoked Dpp-Sep release

Wing imaginal discs from 144-148 h AEL *dpp>dpp-SEP* third instar larvae were dissected and placed in a well containing HL3.1 saline solution on a 24×40 mm coverslip with the peripodial side facing down. Confocal images were taken every 250 ms for 500 cycles. While the images were being taken, HL3.1 saline containing 1 M potassium chloride was added with a long slender gel-loading pipette tip so that the final concentration was 100 mM potassium (Shui et al., 1998). We noted the cycle at which the high potassium solution was added. Control experiments were performed with the addition of normal HL3.1 saline during the imaging. Imaging files were excluded from analysis if the wing disc moved during imaging.

Real-time PCR

Wing discs were isolated from third instar larvae and total RNA extracted using the SV Total RNA Isolation Kit (Promega). Single-stranded cDNA was synthesized using the Superscript III First Strand Synthesis System (Invitrogen). We used a LightCycler 480 with SYBR Green I Master Mix (Roche Diagnostics) and the following primers (5′-3′) to amplify specific transcripts: *Rp49* (*RpL32*), AAGAAGCGCACCAAGCACTTCATC and TCTGTTGTCGATACCCT-TGGGCTT; *KCNJ2*, GATGTGTCACGGATGAATGC and ACTCGCC-ACATCAAACACAG; *Kcnj10*, CAAGGTCTATTACAGCCAGAC and TCCATAGATCCTTGAGGTAGAG; *Ork*, TCCTGCTGCTCATCTTCTA and AGCTCCTCCAGCAGATATT; *Irk2DN*, ACACTATTGCCGCTGCC and CAAATTACGGCGTGTTTGGAGAAC.

Acknowledgements

We thank Dr Lee Niswander for insightful conversations and suggestions; Megan Josey for copy editing; Dr Angeles Ribera and Dr Rosa Moreno for suggestions, discussion, attempts to measure resting membrane potential and explore electrical activity in the wing disc; Dr William J. Betz for writing and assisting in the use of custom MATLAB programs; the University of Colorado Anschutz Medical Campus Advanced Light Microscopy Core and Dr Radu Moldovan for training and use of the 3i Marianis spinning disc confocal; and Matthew Gibson (Stowers Institute) for the Dpp prodomain antibody. The mouse anti-β-galactosidase antibody was developed by Joshua Sanes, and the rat DCAD2 antibody was developed by T. Uemura, and both were obtained from the Developmental Studies Hybridoma Bank created by the NICHD of the NIH and maintained at The University of Iowa, Department of Biology, Iowa City, IA 52242, USA. We thank the Bloomington Drosophila Stock Center for many fly stocks and Dr Michael Levin for the plasmid with cDNA encoding Flag-tagged Kir4.1. We thank the Nancy and Michael Burgermeister Family who donated the funds for the purchase of the Zeiss LSM 780 microscope.

Competing interests

The authors declare no competing or financial interests.

Author contributions

Conceptualization: E.A.B.; Methodology: G.R.D., S.J.P., E.A.B.; Validation: G.R.D.; Formal analysis: G.R.D., S.J.P., E.A.B.; Investigation: G.R.D., S.J.P., E.A.B.; Writing - original draft: E.A.B.; Visualization: G.R.D., S.J.P.; Supervision: E.A.B.; Project administration: E.A.B.; Funding acquisition: E.A.B.

Funding

We thank the National Science Foundation (Integrated Organismal Systems 1354282 to E.A.B.) and National Institutes of Health-National Institute of Dental and Craniofacial Research (1R56DE025311-01 to E.A.B.) for funding. Deposited in PMC for release after 12 months.

Development (2017) 144, 2771-2783 doi:10.1242/dev.146647

Supplementary information

Supplementary information available online at
http://dev.biologists.org/lookup/doi/10.1242/dev.146647.supplemental

References

Adachi-Yamada, T., Fujimura-Kamada, K., Nishida, Y. and Matsumoto, K. (1999). Distortion of proximodistal information causes JNK-dependent apoptosis in Drosophila wing. *Nature* **400**, 166-169.

Adams, D. S., Uzel, S. G. M., Akagi, J., Wlodkowic, D., Andreeva, V., Yelick, P. C., Devitt-Lee, A., Pare, J.-F. and Levin, M. (2016). Bioelectric signalling via potassium channels: a mechanism for craniofacial dysmorphogenesis in KCNJ2-associated Andersen-Tawil Syndrome. *J. Physiol.* **594**, 3245-3270.

Akiyama, T. and Gibson, M. C. (2015). Decapentaplegic and growth control in the developing Drosophila wing. *Nature* **527**, 375-378.

Baines, R. A. (2004). Synaptic strengthening mediated by bone morphogenetic protein-dependent retrograde signaling in the Drosophila CNS. *J. Neurosci.* **24**, 6904-6911.

Bates, E. (2015). Ion channels in development and cancer. *Annu. Rev. Cell Dev. Biol.* **31**, 231-247.

Berke, B., Wittnam, J., McNeill, E., Van Vactor, D. L. and Keshishian, H. (2013). Retrograde BMP signaling at the synapse: a permissive signal for synapse maturation and activity-dependent plasticity. *J. Neurosci.* **33**, 17937-17950.

Bichet, D., Haass, F. A. and Jan, L. Y. (2003). Merging functional studies with structures of inward-rectifier K(+) channels. *Nat. Rev. Neurosci.* **4**, 957-967.

Bokman, S. H. and Ward, W. W. (1981). Renaturation of Aequorea green-fluorescent protein. *Biochem. Biophys. Res. Commun.* **101**, 1372-1380.

Bondy, C. A., Gainer, H. and Russell, J. T. (1987). Effects of stimulus frequency and potassium channel blockade on the secretion of vasopressin and oxytocin from the neurohypophysis. *Neuroendocrinology* **46**, 258-267.

Braun, M., Ramracheya, R., Bengtsson, M., Zhang, Q., Karanauskaite, J., Partridge, C., Johnson, P. R. and Rorsman, P. (2008). Voltage-gated ion channels in human pancreatic beta-cells: electrophysiological characterization and role in insulin secretion. *Diabetes* **57**, 1618-1628.

Brooks, A., Dou, W., Yang, X., Brosnan, T., Pargett, M., Raftery, L. A. and Umulis, D. M. (2012). BMP signaling in wing development: a critical perspective on quantitative image analysis. *FEBS Lett.* **586**, 1942-1952.

Burke, R. and Basler, K. (1996). Dpp receptors are autonomously required for cell proliferation in the entire developing Drosophila wing. *Development* **122**, 2261-2269.

Capdevila, J. and Guerrero, I. (1994). Targeted expression of the signaling molecule decapentaplegic induces pattern duplications and growth alterations in Drosophila wings. *EMBO J.* **13**, 4459-4468.

Chen, Y., Riese, M. J., Killinger, M. A. and Hoffmann, F. M. (1998). A genetic screen for modifiers of Drosophila decapentaplegic signaling identifies mutations in punt, Mothers against dpp and the BMP-7 homologue, 60A. *Development* **125**, 1759-1768.

Cilz, N. I., Kurada, L., Hu, B. and Lei, S. (2014). Dopaminergic modulation of GABAergic transmission in the entorhinal cortex: concerted roles of alpha1 adrenoreceptors, inward rectifier K(+), and T-type Ca(2)(+) channels. *Cereb. Cortex* **24**, 3195-3208.

Contrino, S., Smith, R. N., Butano, D., Carr, A., Hu, F., Lyne, R., Rutherford, K., Kalderimis, A., Sullivan, J., Carbon, S. et al. (2012). modMine: flexible access to modENCODE data. *Nucleic Acids Res.* **40**, D1082-D1088.

Dahal, G. R., Rawson, J., Gassaway, B., Kwok, B., Tong, Y., Ptacek, L. J. and Bates, E. (2012). An inwardly rectifying K+ channel is required for patterning. *Development* **139**, 3653-3664.

de Celis, J. F. (1997). Expression and function of decapentaplegic and thick veins during the differentiation of the veins in the Drosophila wing. *Development* **124**, 1007-1018.

De Celis, J. F. (2003). Pattern formation in the Drosophila wing: the development of the veins. *BioEssays* **25**, 443-451.

Doherty, D., Jan, L. Y. and Jan, Y. N. (1997). The Drosophila neurogenic gene big brain, which encodes a membrane-associated protein, acts cell autonomously and can act synergistically with Notch and Delta. *Development* **124**, 3881-3893.

Döring, F., Wischmeyer, E., Kühnlein, R. P., Jäckle, H. and Karschin, A. (2002). Inwardly rectifying K+ (Kir) channels in Drosophila. A crucial role of cellular milieu factors Kir channel function. *J. Biol. Chem.* **277**, 25554-25561.

Entchev, E. V., Schwabedissen, A. and González-Gaitán, M. (2000). Gradient formation of the TGF-beta homolog Dpp. *Cell* **103**, 981-991.

Gandhi, S. P. and Stevens, C. F. (2003). Three modes of synaptic vesicular recycling revealed by single-vesicle imaging. *Nature* **423**, 607-613.

Hibino, H., Inanobe, A., Furutani, K., Murakami, S., Findlay, I. and Kurachi, Y. (2010). Inwardly rectifying potassium channels: their structure, function, and physiological roles. *Physiol. Rev.* **90**, 291-366.

Hunter, G. L., Crawford, J. M., Genkins, J. Z. and Kiehart, D. P. (2014). Ion channels contribute to the regulation of cell sheet forces during Drosophila dorsal closure. *Development* **141**, 325-334.

James, R. E., Hoover, K. M., Bulgari, D., McLaughlin, C. N., Wilson, C. G., Wharton, K. A., Levitan, E. S. and Broihier, H. T. (2014). Crimpy enables discrimination of presynaptic and postsynaptic pools of a BMP at the Drosophila neuromuscular junction. *Dev. Cell* **31**, 586-598.

Jan, L. Y. and Jan, Y. N. (1976). L-glutamate as an excitatory transmitter at the Drosophila larval neuromuscular junction. *J. Physiol.* **262**, 215-236.

Klebes, A., Biehs, B., Cifuentes, F. and Kornberg, T. B. (2002). Expression profiling of Drosophila imaginal discs. *Genome Biol.* **3**, research0038.

Kneen, M., Farinas, J., Li, Y. and Verkman, A. S. (1998). Green fluorescent protein as a noninvasive intracellular pH indicator. *Biophys. J.* **74**, 1591-1599.

Letsou, A., Arora, K., Wrana, J. L., Simin, K., Twombly, V., Jamal, J., Staehling-Hampton, K., Hoffmann, F. M., Gelbart, W. M., Massagué, J. et al. (1995). Drosophila Dpp signaling is mediated by the punt gene product: a dual ligand-binding type II receptor of the TGF beta receptor family. *Cell* **80**, 899-908.

Levin, M. (2012). Molecular bioelectricity in developmental biology: new tools and recent discoveries: control of cell behavior and pattern formation by transmembrane potential gradients. *BioEssays* **34**, 205-217.

Levin, M. (2014a). Endogenous bioelectrical networks store non-genetic patterning information during development and regeneration. *J. Physiol.* **592**, 2295-2305.

Levin, M. (2014b). Molecular bioelectricity: how endogenous voltage potentials control cell behavior and instruct pattern regulation in vivo. *Mol. Biol. Cell* **25**, 3835-3850.

Luan, Z. and Li, H. S. (2012). Inwardly rectifying potassium channels in Drosophila. *Sheng Li Xue Bao* **64**, 515-519.

MacLean, S. J., Andrews, B. C. and Verheyen, E. M. (2002). Characterization of Dir: a putative potassium inward rectifying channel in Drosophila. *Mech. Dev.* **116**, 193-197.

Maduzia, L. L. and Padgett, R. W. (1997). Drosophila MAD, a member of the Smad family, translocates to the nucleus upon stimulation of the dpp pathway. *Biochem. Biophys. Res. Commun.* **238**, 595-598.

Miesenbock, G., De Angelis, D. A. and Rothman, J. E. (1998). Visualizing secretion and synaptic transmission with pH-sensitive green fluorescent proteins. *Nature* **394**, 192-195.

Misler, S., Barnett, D. W., Gillis, K. D. and Pressel, D. M. (1992). Electrophysiology of stimulus-secretion coupling in human beta-cells. *Diabetes* **41**, 1221-1228.

Nellen, D., Affolter, M. and Basler, K. (1994). Receptor serine/threonine kinases implicated in the control of Drosophila body pattern by decapentaplegic. *Cell* **78**, 225-237.

Nellen, D., Burke, R., Struhl, G. and Basler, K. (1996). Direct and long-range action of a DPP morphogen gradient. *Cell* **85**, 357-368.

Newfeld, S. J., Mehra, A., Singer, M. A., Wrana, J. L., Attisano, L. and Gelbart, W. M. (1997). Mothers against dpp participates in a DDP/TGF-beta responsive serine-threonine kinase signal transduction cascade. *Development* **124**, 3167-3176.

O'Connor, M. B., Umulis, D., Othmer, H. G. and Blair, S. S. (2006). Shaping BMP morphogen gradients in the Drosophila embryo and pupal wing. *Development* **133**, 183-193.

Pai, V. P., Aw, S., Shomrat, T., Lemire, J. M. and Levin, M. (2012). Transmembrane voltage potential controls embryonic eye patterning in Xenopus laevis. *Development* **139**, 313-323.

Paroutis, P., Touret, N. and Grinstein, S. (2004). The pH of the secretory pathway: measurement, determinants, and regulation. *Physiology (Bethesda)* **19**, 207-215.

Plaster, N. M., Tawil, R., Tristani-Firouzi, M., Canún, S., Bendahhou, S., Tsunoda, A., Donaldson, M. R., Iannaccone, S. T., Brunt, E., Barohn, R. et al. (2001). Mutations in Kir2.1 cause the developmental and episodic electrical phenotypes of Andersen's syndrome. *Cell* **105**, 511-519.

Posakony, L. G., Raftery, L. A. and Gelbart, W. M. (1990). Wing formation in Drosophila melanogaster requires decapentaplegic gene function along the anterior-posterior compartment boundary. *Mech. Dev.* **33**, 69-82.

Raftery, L. A. and Sutherland, D. J. (1999). TGF-beta family signal transduction in Drosophila development: from Mad to Smads. *Dev. Biol.* **210**, 251-268.

Raftery, L. A., Twombly, V., Wharton, K. and Gelbart, W. M. (1995). Genetic screens to identify elements of the decapentaplegic signaling pathway in Drosophila. *Genetics* **139**, 241-254.

Raftery, L. A. and Umulis, D. M. (2012). Regulation of BMP activity and range in Drosophila wing development. *Curr. Opin. Cell Biol.* **24**, 158-165.

Ralston, A. and Blair, S. S. (2005). Long-range Dpp signaling is regulated to restrict BMP signaling to a crossvein competent zone. *Dev. Biol.* **280**, 187-200.

Ranade, S. S., Qiu, Z., Woo, S.-H., Hur, S. S., Murthy, S. E., Cahalan, S. M., Xu, J., Mathur, J., Bandell, M., Coste, B. et al. (2014). Piezo1, a mechanically activated ion channel, is required for vascular development in mice. *Proc. Natl. Acad. Sci. USA* **111**, 10347-10352.

Riz, M., Braun, M., Wu, X. and Pedersen, M. G. (2015). Inwardly rectifying Kir2.1 currents in human beta-cells control electrical activity: characterisation and mathematical modelling. *Biochem. Biophys. Res. Commun.* **459**, 284-287.

Rorsman, P. and Braun, M. (2013). Regulation of insulin secretion in human pancreatic islets. *Annu. Rev. Physiol.* **75**, 155-179.

Roy, S., Huang, H., Liu, S. and Kornberg, T. B. (2014). Cytoneme-mediated contact-dependent transport of the Drosophila decapentaplegic signaling protein. *Science* **343**, 1244624.

Development (2017) 144, 2771-2783 doi:10.1242/dev.146647

Sekelsky, J. J., Newfeld, S. J., Raftery, L. A., Chartoff, E. H. and Gelbart, W. M. (1995). Genetic characterization and cloning of mothers against dpp, a gene required for decapentaplegic function in Drosophila melanogaster. *Genetics* **139**, 1347-1358.

Shimmi, O., Ralston, A., Blair, S. S. and O'Connor, M. B. (2005). The crossveinless gene encodes a new member of the Twisted gastrulation family of BMP-binding proteins which, with Short gastrulation, promotes BMP signaling in the crossveins of the Drosophila wing. *Dev. Biol.* **282**, 70-83.

Shui, H. A., Peng, Y. I. and Tsai, F. F. (1998). Recovery of high potassium-evoked dopamine release after depolarization challenge in the striatum of young and old male rats. *Neurosci. Lett.* **257**, 1-4.

Sorre, B., Warmflash, A., Brivanlou, A. H. and Siggia, E. D. (2014). Encoding of temporal signals by the TGF-beta pathway and implications for embryonic patterning. *Dev. Cell* **30**, 334-342.

Spencer, F. A., Hoffmann, F. M. and Gelbart, W. M. (1982). Decapentaplegic: a gene complex affecting morphogenesis in Drosophila melanogaster. *Cell* **28**, 451-461.

Splawski, I., Timothy, K. W., Sharpe, L. M., Decher, N., Kumar, P., Bloise, R., Napolitano, C., Schwartz, P. J., Joseph, R. M., Condouris, K. et al. (2004). Ca (V)1.2 calcium channel dysfunction causes a multisystem disorder including arrhythmia and autism. *Cell* **119**, 19-31.

Stewart, B. A., Atwood, H. L., Renger, J. J., Wang, J. and Wu, C. F. (1994). Improved stability of Drosophila larval neuromuscular preparations in haemolymph-like physiological solutions. *J. Comp. Physiol. A* **175**, 179-191.

Strigini, M. and Cohen, S. M. (2000). Wingless gradient formation in the Drosophila wing. *Curr. Biol.* **10**, 293-300.

Sulkowski, M., Kim, Y.-J. and Serpe, M. (2014). Postsynaptic glutamate receptors regulate local BMP signaling at the Drosophila neuromuscular junction. *Development* **141**, 436-447.

Swapna, I. and Borodinsky, L. N. (2012). Interplay between electrical activity and bone morphogenetic protein signaling regulates spinal neuron differentiation. *Proc. Natl. Acad. Sci. USA* **109**, 16336-16341.

Teleman, A. A. and Cohen, S. M. (2000). Dpp gradient formation in the Drosophila wing imaginal disc. *Cell* **103**, 971-980.

Tristani-Firouzi, M., Jensen, J. L., Donaldson, M. R., Sansone, V., Meola, G., Hahn, A., Bendahhou, S., Kwiecinski, H., Fidzianska, A., Plaster, N. et al. (2002). Functional and clinical characterization of KCNJ2 mutations associated with LQT7 (Andersen syndrome). *J. Clin. Invest.* **110**, 381-388.

Tseng, A.-S., Beane, W. S., Lemire, J. M., Masi, A. and Levin, M. (2010). Induction of vertebrate regeneration by a transient sodium current. *J. Neurosci.* **30**, 13192-13200.

Vaca, L., Licea, A. and Possani, L. D. (1996). Modulation of cell membrane potential in cultured vascular endothelium. *Am. J. Physiol.* **270**, C819-C824.

Varga, Z., Juhász, T., Matta, C., Fodor, J., Katona, E., Bartok, A., Oláh, T., Sebe, A., Csernoch, L., Panyi, G. et al. (2011). Switch of voltage-gated K+ channel expression in the plasma membrane of chondrogenic cells affects cytosolic Ca2+-oscillations and cartilage formation. *PLoS ONE* **6**, e27957.

Ward, W. W. and Bokman, S. H. (1982). Reversible denaturation of Aequorea green-fluorescent protein: physical separation and characterization of the renatured protein. *Biochemistry* **21**, 4535-4540.

Wiersdorff, V., Lecuit, T., Cohen, S. M. and Mlodzik, M. (1996). Mad acts downstream of Dpp receptors, revealing a differential requirement for dpp signaling in initiation and propagation of morphogenesis in the Drosophila eye. *Development* **122**, 2153-2162.

Xiao, L., Michalski, N., Kronander, E., Gjoni, E., Genoud, C., Knott, G. and Schneggenburger, R. (2013). BMP signaling specifies the development of a large and fast CNS synapse. *Nat. Neurosci.* **16**, 856-864.

Yoon, G., Oberoi, S., Tristani-Firouzi, M., Etheridge, S. P., Quitania, L., Kramer, J. H., Miller, B. L., Fu, Y. H. and Ptáček, L. J. (2006). Andersen-Tawil syndrome: prospective cohort analysis and expansion of the phenotype. *Am. J. Med. Genet. A* **140**, 312-321.

Zaritsky, J. J., Eckman, D. M., Wellman, G. C., Nelson, M. T. and Schwarz, T. L. (2000). Targeted disruption of Kir2.1 and Kir2.2 genes reveals the essential role of the inwardly rectifying K(+) current in K(+)-mediated vasodilation. *Circ. Res.* **87**, 160-166.

Zecca, M., Basler, K. and Struhl, G. (1995). Sequential organizing activities of engrailed, hedgehog and decapentaplegic in the Drosophila wing. *Development* **121**, 2265-2278.

Zeng, Y. A., Rahnama, M., Wang, S., Sosu-Sedzorme, W. and Verheyen, E. M. (2007). Drosophila Nemo antagonizes BMP signaling by phosphorylation of Mad and inhibition of its nuclear accumulation. *Development* **134**, 2061-2071.

Supplemental Information

Figure S1

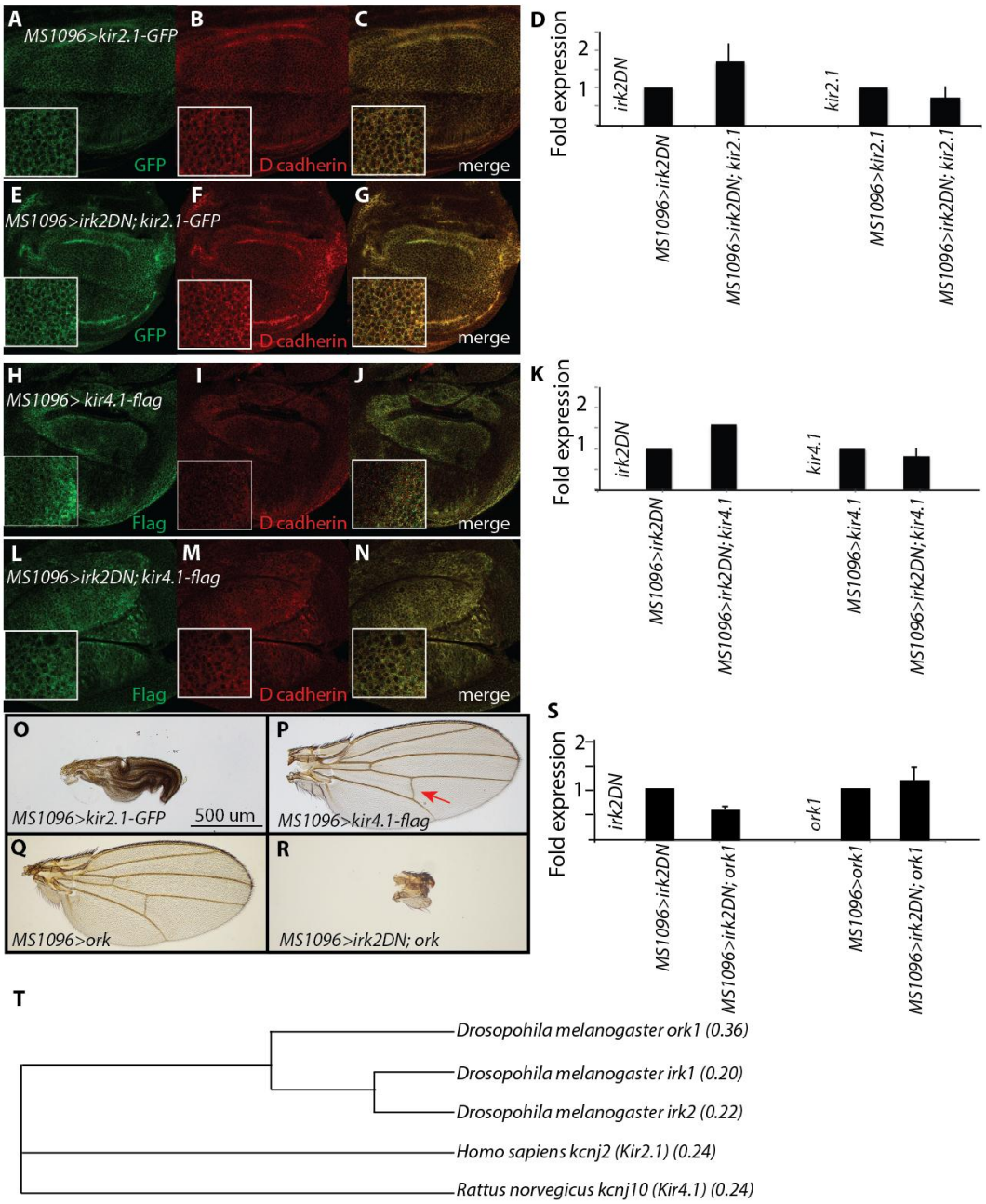

Figure S1. Kir2.1-GFP and Kir4.1-Flag localize to the cellular membrane in third instar larval wing discs.

(**A, B, C**) *MS1096>kcnj2-GFP* wing discs co-stained with anti-GFP (green, **A**) and anti-D-cadherin (red, **B**) show that Kir2.1 localizes to the membrane (merged, **C**).

(**D)** Q-RT-PCR quantification of *irk2DN* and *kcnj2* in *MS1096>irk2DN, MS1096>irk2DN; kcnj2-GFP,* and *MS1096> kcnj2-GFP* wing discs shows that transgenes are expressed.

(E, F, G) *MS1096>irk2DN; kcnj2-GFP* wing discs are co-stained with anti-GFP (green, **E**) and anti-D-cadherin (red, **F**) show localization of Kir2.1 to the membrane is not affected by expression of Irk2DN (merged, **G**).

(**H, I, J)** *MS1096>kcnj10-Flag* co-stained with anti-Flag (green, **H**) and anti-D-cadherin (red, **I**) show localization of Kir4.1 to the membrane (merged, **J**).

(**K**) Q-RT-PCR quantification of *irk2DN* and *kcnj10* in *MS1096>irk2DN, MS1096>irk2DN; kcnj10-Flag,* and *MS1096> kcnj10-Flag* wing discs shows that transgenes are expressed.

(**L, M, N**) *MS1096>irk2DN; kcnj10-Flag* co-stained with anti-Flag (green, **L**) and anti-D-cadherin (red, **M**) show localization of Kir4.1 to the membrane is not affected by expression of Irk2DN (merged, **N**).

(O) Overexpression of Kir2.1 (*MS1096>kcnj2-gfp*) alone prevents the wing from expanding properly, so wing patterning defects can not be quantified.

(P) Overexpression of Kir4.1 (*MS1096>kcnj10-flag)* alone results in an increase in wing size with only minor wing venation defects (red arrow).

(Q) Overexpression of Ork (*MS1096>ork*) alone results in an increase in wing size with only minor wing venation defects.

(R) Overexpression of Ork with *irk2DN (ms1096>irk2DN;ork)* fails to rescue wing defects caused by Irk2DN.

(S) Q-RT-PCR quantification of *irk2DN* and *ork* in *MS1096>irk2DN, MS1096>irk2DN; ork,* and *MS1096> ork* wing discs shows that transgenes are expressed.

(T) A phylogenetic tree shows the relationship between *Homo sapiens* Kir2.1 (*kcnj2)*, *Rattus norvegicus* Kir4.1 (*kcnj10*), *Drosophila melanogaster* Irk1, *Drosophila melanogaster* Irk2, and *Drosophila melanogaster* Ork.

Figure S2

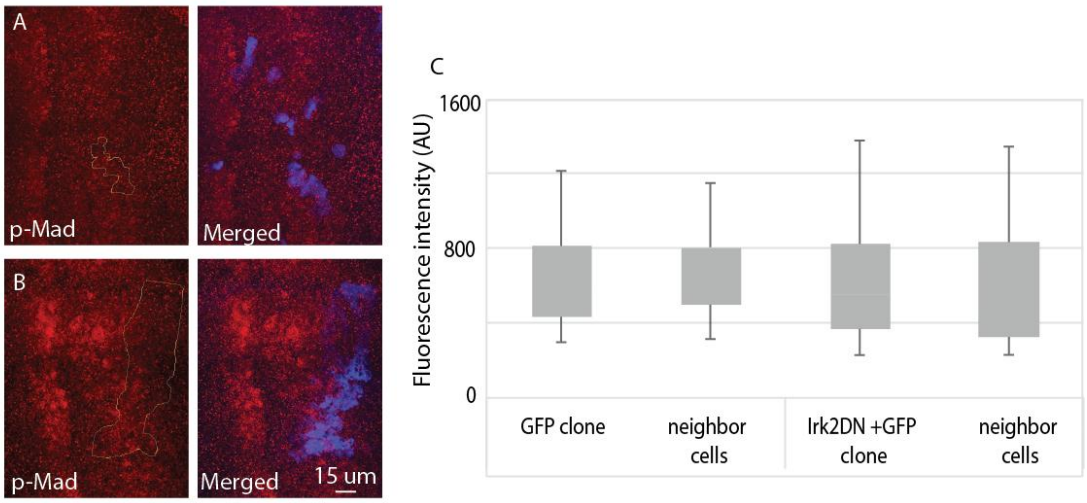

Figure S2. Clones expressing GFP with or without *irk2DN* do not affect anti-p-Mad fluorescence intensity.

(A) A representative example (out of 39 clones) that express only GFP in third instar larval wing discs co-stained with antibodies against p-Mad (red) and GFP (blue).

(**B**) A representative example (out of 38 clones) that express *irk2DN* and *GFP* in third instar larval wing discs co-stained with antibodies against p-Mad (red) and GFP (blue). P-Mad alone is shown on the left, and both green and red channels are merged in the right column. The scale bar is 15 um.

(**C**) The graph shows quantification of p-Mad immuno-fluorescence of cells within clones compared to neighboring cells outside of clones. There is no significant difference between p-Mad immuno-fluorescence for GFP clones (n=39 clones, p=0.94 t-test) or for Irk2DN expressing clones (n=38 clones, p=0.87 t-test). Error bars are standard error of the mean.

Figure S3

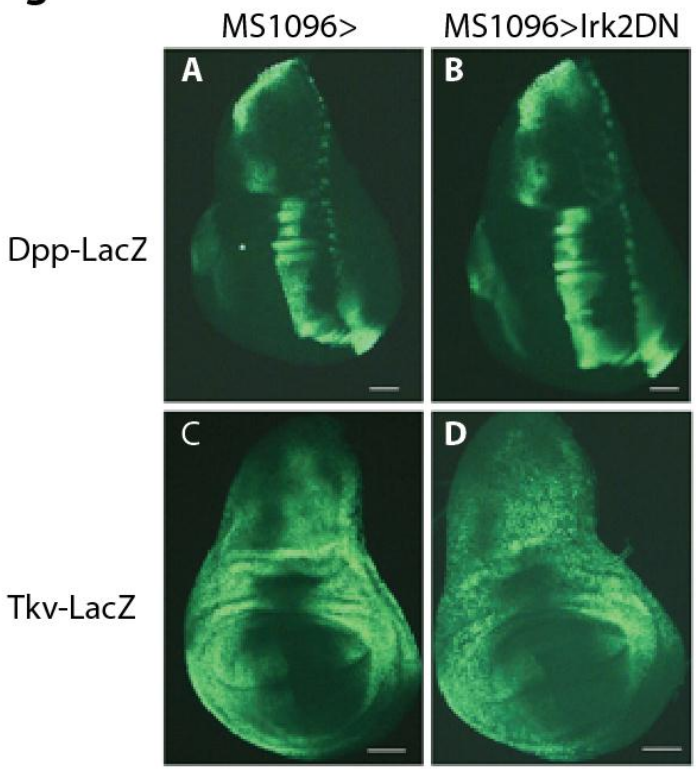

Figure S3. Irk2DN does not significantly affect expression of Tkv, Dpp, or Dally. All discs are stained with anti-LacZ antibody.

(**A, B)** *MS1096>; dpp-LacZ* wing discs (A) stained with anti-LacZ antibody are not significantly different from *dpp-LacZ; MS1096>irk2DN13* (B).

(**C, D**) *MS1096>;tkv-LacZ* wing discs (**C)** are compared Tkv-LacZ; MS1096> Irk2DN13 wing discs (**D).** The scale bars are 100 um for all panels.

Figure S4

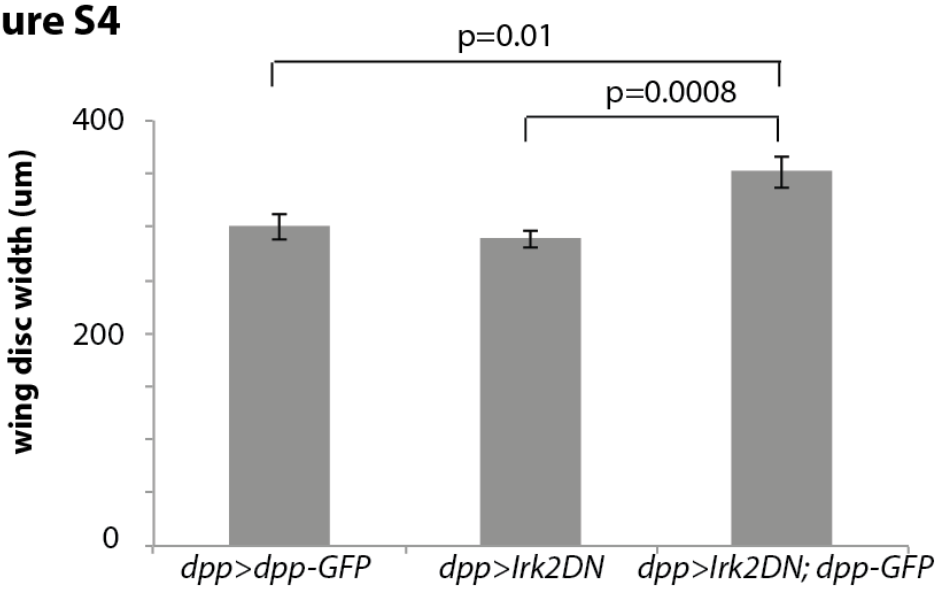

Figure S4. Inhibition of Irk channels in the Dpp-producing cells increases the size of the wing disc. Wing discs were measured at the widest region of the disc, perpendicular to the AP boundary. Error bars are standard error of the mean.

Figure S5

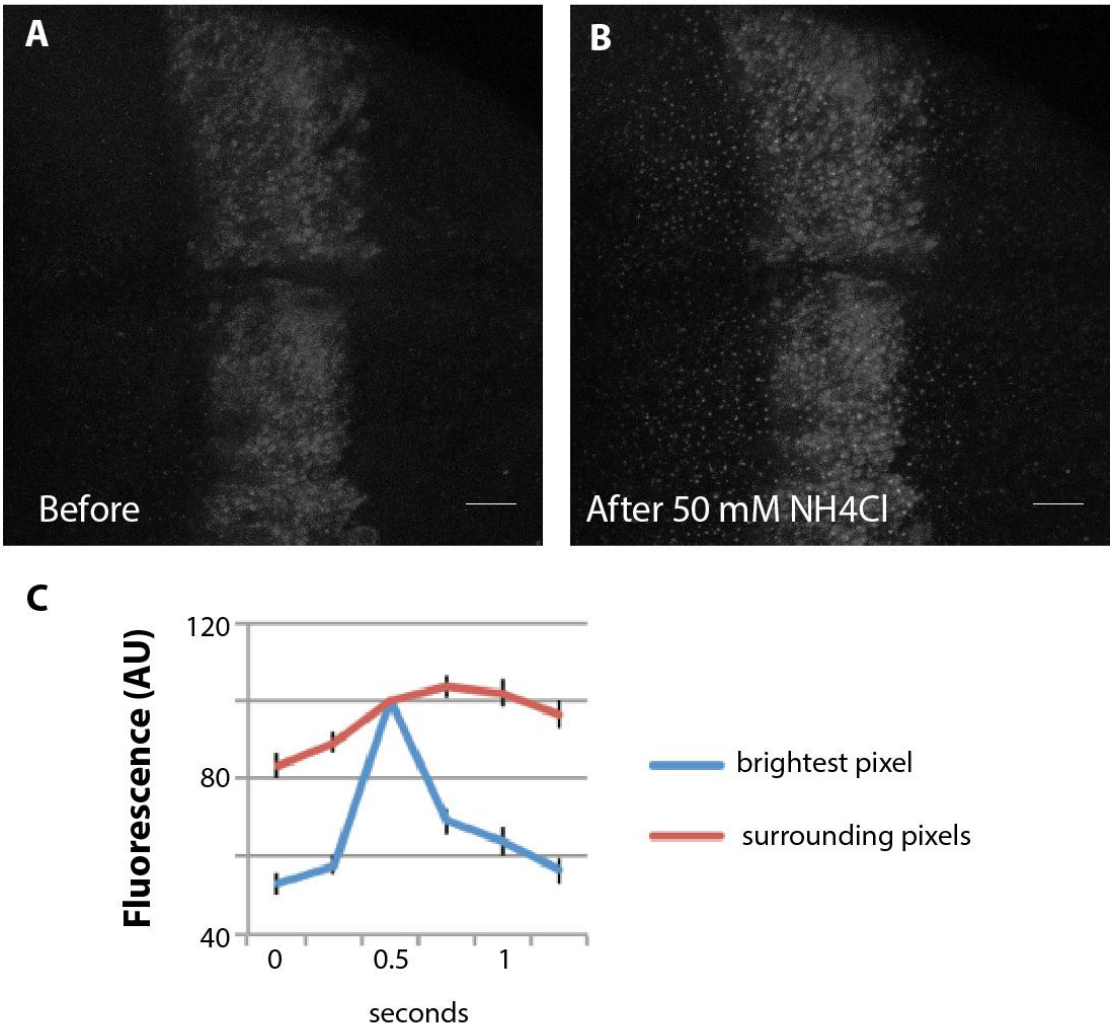

Figure S5. GFP is quenched in vesicles of the wing disc and fluorescence spreads upon release.

(A) Dpp-GFP fluorescence is quenched in a *dpp>dpp-GFP* wing disc before addition of 50 mM ammonium chloride.

(B) Image of the same *dpp>dpp-GFP* wing disc one minute after addition of 50 mM ammonium chloride showing that the fluorescence is brighter.

(C) Quantification of fluorescence in arbitrary units (AU) in one pixel (blue) and surrounding 8 pixels (red) 0.25 and 0.5 seconds before and 0.25 and 0.5 seconds after the brightest pixel appears.

Figure S6

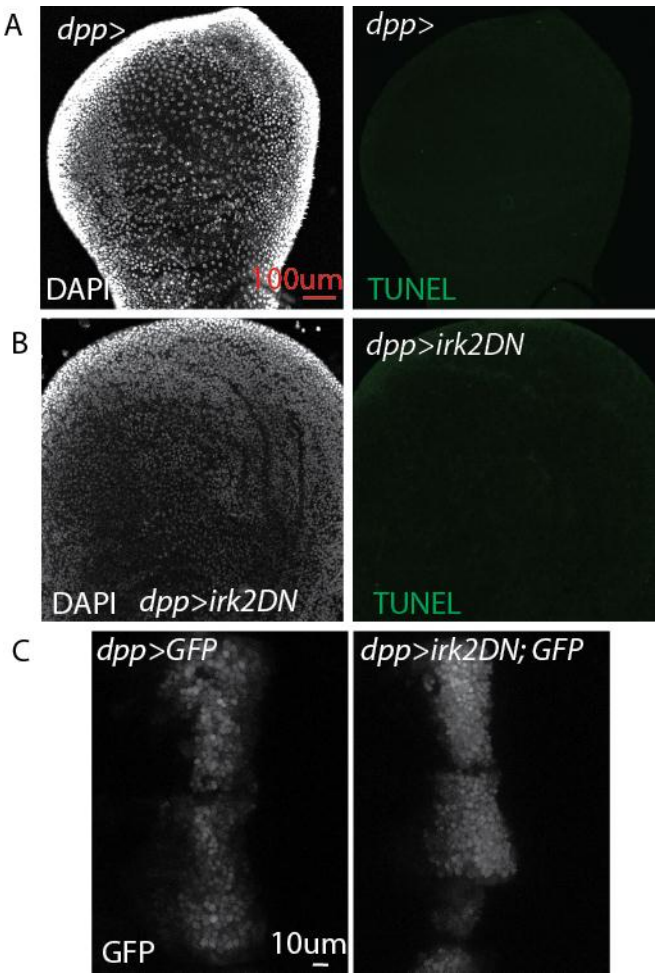

Figure S6. Apoptosis is not detected in *dpp>GFP and dpp>irk2DN* wing discs.

(A) An image of a dpp> wing disc stained with DAPI to identify nuclei (left) and TUNEL to identify apoptotic cells (right) shows that no apoptosis is detected in *dpp>* wing discs at this stage. The scale bar is 100 um and applies to panels A and B.

(B) An image of a dpp>irk2DN wing disc stained with DAPI to identify nuclei (left) and TUNEL to identify apoptotic cells (right) shows that no apoptotic cells are detected in *dpp>irk2DN* wing discs at this stage.

(C) Images of *dpp>GFP* and *dpp>irk2DN;GFP* wing discs show that GFP fluorescence is not decreased in *dpp>irk2DN;GFP* wing discs.